A synthetic float analysis of upper-limb meridional overturning circulation interior ocean pathways in the tropical/subtropical Atlantic

G. R. Halliwell, Jr.[a*], R. H. Weisberg[b], and D. A. Mayer[c&]

[a] Rosenstiel School of Marine and Atmospheric Science, University of Miami, 4600 Rickenbacker Causeway, Miami, Florida, 33149, USA

[b] College of Marine Science, University of South Florida, St. Petersburg, Florida, USA

[c] National Oceanic and Atmospheric Administration, Atlantic Oceanographic and Meteorological Laboratory, Miami, Florida, USA

Synthetic floats are released in an ocean general circulation model to study fluid pathways followed by the upper limb of the meridional overturning circulation from the subtropical South Atlantic to the subtropical North Atlantic. The floats are designed to track this fundamentally three-dimensional, non-isentropic flow while sampling water properties and all terms of the equation governing the vertical component of relative vorticity. The low-resolution ocean simulations demonstrate how upper-limb flow navigates the complex, time-dependent system of wind-driven gyres. Pathways that extend into the interior North Atlantic before entering the Caribbean Sea are emphasized over the more direct western boundary route. A large number of floats are released in the southern hemisphere to verify the importance of such interior pathways in the model and document key events that occur along them. Upper limb water first approaches the equator in a modified inertial western boundary layer. Equatorial processes (visco-inertial boundary layer dynamics, upwelling, heating) are necessary to reset water properties and permit fluid to permanently cross the equator, typically requiring eastward retroflection into the EUC. After upwelling at the equator, fluid that does not advect northward or southward into the interior returns to the western boundary and turns northward in a frictional western boundary layer. The generation of negative relative vorticity by planetary vorticity advection can break the boundary layer constraint and permit retroflection into the NECC near 5°N from late spring through fall. Once in the

* Corresponding author: Tel. 1+305+361-4621, E-mail: ghallwell@rsmas.miami.edu

& Present address: College of Marine Science, University of South Florida, St. Petersburg, Florida, USA

interior, this fluid advects northward into the southern subtropical gyre in a flow governed by Ekman dynamics. There the fluid subducts and advects southwestward to enter the Caribbean Sea under the influence of layered thermocline dynamics. The importance of interior pathways is confirmed although we note that fluid parcels generally take complex paths and frequently make multiple attempts to enter the northern hemisphere or multiple treks around gyres.

1. INTRODUCTION

The overturning circulation of the global ocean exerts an important influence on the storage and redistribution of internal energy within the Earth's climate system. The Atlantic Ocean plays a unique role in this by virtue of the deep water formation that occurs at high latitudes. North Atlantic Deep Water formed near Iceland and Greenland flows southward as a Deep Western Boundary Current that eventually feeds the deep flows of the Indian and Pacific Oceans. This necessitates an upper ocean return flow within the Atlantic basin. The resulting overturning system of cold deep water exiting and warmer surface water entering the North Atlantic is referred to as the Meridional Overturning Circulation (MOC), and the return flow is referred to as the upper-limb of the MOC. The understanding of upper-limb pathways and associated water mass modifications that occur en route is important because these will influence the vertical stability of the flow that eventually reaches the subpolar North Atlantic. This could then influence the deep water formation rate and thus the strength of the MOC and associated net northward heat flux.

The upper-limb of the MOC cannot follow a simple path from the South Atlantic to the North Atlantic because of the angular momentum constraint imposed by the Earth's rotation and the resulting system of wind-driven gyres. Of particular interest to the present study are the paths taken by fluid parcels as they navigate from the South Atlantic subtropical gyre, across the equatorial and tropical gyres, and then into the North Atlantic subtropical gyre. It is known from previous studies that the circulation connecting these gyres must be fully three-dimensional and seasonally varying. The equator is a location of special concern because of strong upwelling and surface heating. Western boundary processes are also important. Unlike the Gulf Stream that closes the North Atlantic subtropical gyre over a continuous meridional extent of some 15 degrees latitude, the western boundary currents of the equatorial and tropical gyres generally extend along less than 5 degrees latitude and flow in opposite directions. *Munk* [1950] suggested that these features should not even be called gyres for these reasons. Moreover, these western boundary currents vary seasonally, and the North Brazil Current (NBC) that closes the equatorial gyre is unstable during the time of year when these gyres are most developed (late spring through fall). During this time, the southeastward western boundary flow of the tropical gyre acts to block the NBC, so a large fraction of the NBC retroflects and flows eastward to become the North Equatorial Countercurrent (NECC). The retroflection is unstable and eddies occasionally pinch off and

migrate northward carrying a fraction of the upper-limb fluid. In addition to the gyres, upper-ocean flow also includes subtropical overturning cells that return water subducted in the subtropical North and South Atlantic back toward the equator [*Malanotte-Rizzoli et al.*, 2000; *Lazar et al.*, 2002).

These and other processes provide a multitude of possible upper-limb pathways. The observational record is presently inadequate to accurately map these pathways, quantify the mass fluxes associated with them, understand the controlling dynamics, and quantify the water mass modifications that occur. Numerical model experiments are needed, and while ocean general circulation models are imperfect, they are sufficiently realistic to begin identifying and understanding the physical processes that govern upper-limb pathways, and to help guide observational strategies.

Recent improvements in numerical models, including the development of the HYbrid-Coordinate Ocean Model (HYCOM) [*Bleck,* 2002; *Halliwell,* 2003] with the addition of improved synthetic float/drifter technology, allow us to pursue a new model analysis of upper-limb pathways. We identify upper-limb pathways, along with important dynamical and thermodynamical processes that control them, in a low-resolution HYCOM simulation of the Atlantic Ocean. Because of the low model resolution, the western boundary pathway and the influence of NBC rings are not a focus of the present study. Instead, specific attention is given to fluid parcels that follow interior pathways as governed by processes resolved in the low-resolution model. In particular, upper-limb water that enters the interior via the NECC before joining the North Atlantic subtropical gyre circulation is studied in the most detail. Thermodynamical variables, along with terms of the relative vorticity balance, are interpolated to the floats to aid in our understanding of the governing processes. In doing this, we demonstrate the importance of five key processes that govern interior upper-limb pathways: (1) boundary layer dynamics, including western, surface, and equatorial boundary layers; (2) equatorial upwelling and the associated water mass modifications; (3) seasonal variability of the wind-driven tropical and equatorial gyres; (4) interior Ekman wind-drift; and (5) subtropical subduction. These processes change or reset fluid parcel vorticity in ways that permit upper-limb fluid to cross the equator and transit between gyres. Despite the limitations of low-resolution simulations, the insights gained are scientifically interesting and will aid in the interpretation of observations and in the design of high-resolution simulations.

In carrying out these analyses, we validate the use of synthetic three-dimensional Lagrangian (particle-following) floats as a tool for numerical circulation model analysis of thermohaline circulation pathways. The feasibility of using model floats to track fluid pathways have been demonstrated in earlier studies. For example, *Fratantoni* [1996] seeded the Miami Isopycnic-Coordinate Ocean Model (MICOM) with isopycnic floats to study flow pathways in the tropical Atlantic. *Malanotte-Rizzoli et al.* [2000] and *Lazar et al.* [2002] used isopycnic floats to track fluid pathways from the subtropics to the equator, seeding the flow after it had subducted. However, there are limitations to using isopycnic floats in models to track flows that are fundamentally non-isentropic. *Harper* [2000] seeded subduction regions of the global ocean near the surface

with three-dimensional particle-following floats and successfully tracked fluid pathways before and after subduction. The present study demonstrates the importance of using three-dimensional particle-following floats to map pathways of upper-limb MOC fluid as it flows from the subtropical South Atlantic across the equator and into the North Atlantic subtropical gyre.

2. BACKGROUND AND GOALS

The tropical Atlantic Ocean circulation has been the subject of studies ranging from major multi-national expeditions to individual efforts. A selected few papers provide the essential backdrop for our work. We begin with the analysis of IGY hydrographic sections by *Roemmich* [1983] in which estimates of the zonally integrated mass and internal energy transports are presented at several latitudes based on geostrophic and Ekman dynamics. These quantify the MOC and show that the upper-limb transports must transition from primarily within the thermocline layer upon approaching the equator from the South Atlantic to the mixed layer upon leaving the equator to the North Atlantic. This can only occur through water mass modification as fluid is upwelled and heated. *Philander and Pacanowski* [1986a; 1986b] model the seasonally varying circulation along with meridional mass and internal energy fluxes. These analyses demonstrate a dependence upon the gyres' seasonally varying dynamic topography [*e.g., Garzoli and Katz*, 1983; *Katz,* 1987] for the storage and release of the internal energy accumulated as a result of the MOC and surface heat flux.

On the basis of this information, plus a seasonal Sverdrup streamfunction analysis, *Mayer and Weisberg* [1993] hypothesize a composite annual cycle to accommodate across-equator and inter-gyre exchange in a manner consistent with a cyclonic tropical gyre negating a continuous western boundary current (NBC). The hypothesis depends on different processes acting at different locations during different times of year to influence the upper-limb transports (e.g. inertial boundary layer dynamics at the equatorial western boundary during late spring/summer and interior Ekman transports near the NECC ridge/trough region during late fall/winter). These processes force a significant fraction of upper limb fluid to flow into the ocean interior within the NECC during late spring through fall when internal energy is stored at that latitude, and to then flow northward in the near-surface wind-drift during the following winter when internal energy is released to higher latitudes. Since key processes governing this interior pathway hypothesis are reproducible in low-resolution ocean simulations, verification of this hypothesis is a particular focus of the present analysis. According to *Schott et al.* [1998], up to one-quarter of the upper limb flow on annual average follows a pathway that extends into the interior North Atlantic, either flowing eastward in the NECC or flowing directly northward from the equator. Based on water property analysis, *Schmitz and Richardson* [1991] and *Schmitz and McCartney* [1993] also find that upper-limb pathways must include an interior route. Eulerian analysis of Atlantic Ocean simulations by the Navy Layered Ocean Model [*Fratantoni et al.*, 2000] has recently been

employed to estimate upper-limb fluxes following different pathways. That study also demonstrates the likely importance of interior pathways.

Annual mean flux estimates along different pathways consistent with these and other studies are summarized in Figure 1. We follow the observational synthesis by *Schott et al.* [1998], who subdivide the MOC upper-limb flow approaching the equator from the southern hemisphere into three vertical layers: surface ($\sigma_\theta < 24.5$), thermocline ($24.5 < \sigma_\theta < 26.8$), and intermediate ($\sigma_\theta > 26.8$ and above 1000 m). The intermediate layer contributes a substantial fraction of the upper-limb flow, but it follows the western boundary and does not contribute significantly to interior North Atlantic pathways. The thermocline layer flow does contribute to interior pathways, but only after upwelling into the surface layer at the equator, consistent with the asymmetry described by *Roemmich* [1983]. The 4 Sv annual mean northward surface layer flow in the interior, which represents the interior pathway flows of interest to this study, consists of about equal contributions of fluid entering from the western boundary region via the NECC

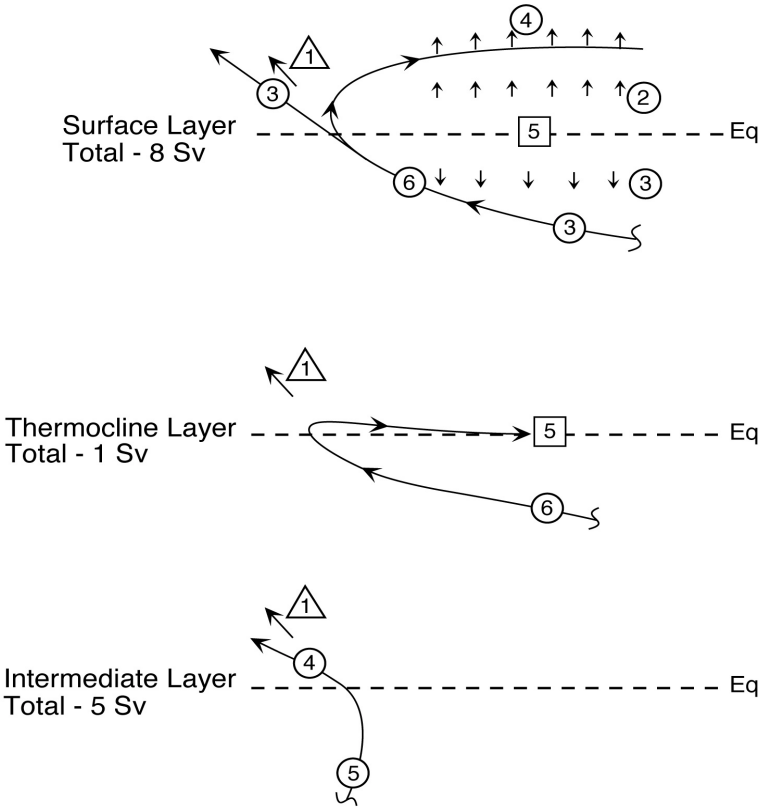

Figure 1. Schematic diagram of the upper limb transport contribution of fluid approaching the equator from the south within three vertical layers: surface layer (σ_θ<24.5, top), thermocline layer (24.5<σ_θ<26.8, middle), and intermediate layer (σ_θ>26.8 and above 1000 m, bottom). Circled numbers are horizontal fluxes in Sverdrups. Numbers in squares indicate vertical upwelling fluxes while numbers in triangles indicate horizontal fluxes within North Brazil Current eddies. All fluxes represent annual averages.

and advecting directly northward from the equator. This interior surface layer flow consists of a mixture of both surface and thermocline water that approaches the equator from the south.

Although we use this schematic to guide our analysis, we do not attempt to quantitatively verify these flux estimates with a model whose resolution does not permit that. We do, however, suggest qualitative modifications to the Figure 1 scenario. Our primary focus is on processes that are not critically dependent on model resolution, specifically the five key processes outlined in the Introduction, as pertinent to governing upper-limb pathways and validating the interior pathways hypothesis.

3. ANALYSIS PROCEDURES

3.1. The numerical model

HYCOM is a primitive equation ocean general circulation model that was developed from MICOM by extending the capabilities of the MICOM vertical coordinate grid. Advantages of isopycnic coordinates in the open, stratified ocean include the absence of spurious numerical diapycnal mixing and efficient resolution of baroclinic structure. However, isopycnic coordinates provide little or no resolution in regions of weak stratification such as the surface mixed layer while terrain-following (sigma) coordinates are considered to be the best choice in shallow water regions. To remedy these deficiencies, HYCOM was equipped with a hybrid vertical coordinate. In the open-ocean, the vertical grid consists of fixed level (pressure) coordinates confined close to the ocean surface that transition smoothly to isopycnic coordinates with increasing depth. In practice, the depth range of the transition region is set as a compromise between preserving the advantages of isopycnic coordinates throughout as much of the water column as possible while resolving the surface boundary layer with pressure coordinates throughout as much of the year as possible. A perfect compromise is not possible because of the large annual cycle of surface boundary layer thickness at high

Table 1
Reference σ_2 for each model layer and user-specified the minimum thickness of each layer maintained by the hybrid coordinate adjustment algorithm.

Layer No.	1	2	3	4	5	6	7	8	9
Ref. σ_2	28.50	29.30	30.10	30.90	31.70	32.51	33.32	34.04	34.75
Min. Thick.	6.0	6.8	7.8	8.9	10.1	11.6	13.2	15.0	15.0
Layer No.	10	11	12	13	14	15	16	17	18
Ref. σ_2	35.29	35.71	36.03	36.27	36.45	36.60	36.72	36.81	36.87
Min. Thick.	15.0	15.0	15.0	15.0	15.0	15.0	15.0	15.0	15.0
Layer No.	19	20	21	22	23	24	25		
Ref. σ_2	36.93	36.99	37.05	37.11	37.17	37.23	37.29		
Min. Thick.	15.0	15.0	15.0	15.0	15.0	15.0	15.0		

latitudes. The isopycnic coordinates are allowed to collapse to zero thickness at the bottom. The HYCOM vertical grid is also designed to transition from level and isopycnic coordinates in the ocean interior to sigma coordinates in shallow water regions. Since we analyze a low-resolution, open-ocean simulation, this coastal coordinate transition does not play a significant role in the present study.

With hybrid coordinates providing vertical resolution in the mixed layer, it is possible to include more sophisticated turbulence closure schemes in HYCOM than was possible in MICOM, which used the slab Kraus-Turner model. Model simulations reported here use the non-slab, nonlocal K-Profile Parameterization (KPP) vertical mixing algorithm of Large et al. [1994] that provides vertical mixing from surface to bottom. Details of the hybrid vertical coordinate algorithm are presented in Bleck [2002] and information on the full suite of vertical mixing schemes included in HYCOM is given in Halliwell [2003].

For the present analysis, seasonal Atlantic Ocean circulation variability is simulated in a domain from 30°S to 70°N. The horizontal grid consists of squares on a Mercator projection with zonal resolution of 1.4 degrees and meridional resolution of 1.4 $\cos\phi$ degrees, where ϕ is latitude. The hybrid vertical grid consists of 25 layers. The isopycnic vertical coordinate is density referenced to a pressure of 2000 dbar. The discretized reference density in σ_2 units, along with the specified minimum thickness enforced by the hybrid vertical coordinate adjustment algorithm, are presented for each model layer in Table 1. Reference densities for the top three layers are chosen to be smaller than the least dense water present anywhere in the Atlantic so that at least three level coordinate layers are always present at the surface to provide important nearsurface vertical resolution for the mixed layer model. The influence of potential density anomalies on seawater compressibility (thermobaricity) is included [Sun et al., 1999]. The buoyancy anomalies produced by thermobaricity result in pressure gradient anomalies that, although small, significantly influence the representation of deep thermohaline circulation such as the MOC in long climate integrations.

The model is driven by monthly climatological surface fields of vector wind stress, wind speed, u^*, air temperature, air specific humidity, net shortwave radiation, net longwave radiation, and precipitation, all derived from the 1979-2000 NCEP/DOE atmospheric reanalysis product [*Kanamitsu et al.*, 2002]. This reanalysis uses the same assimilation system as the original NCEP/NCAR reanalysis [*Kalnay et al,* 1996], but with all known errors corrected. Evaporation and surface turbulent heat flux components are computed during model run time using bulk formula with the drag coefficient parameterizations of *Kara et al.* [2000a]. For northern and southern boundary conditions, model fields are relaxed to World Ocean Atlas 1994 (WOA94) climatology [*Levitus and Boyer,* 1994; *Levitus et al.*, 1994] within six grid points of the boundary. The inverse relaxation time scale decreases linearly away from the boundaries. Although precipitation is provided as a forcing field, surface salinity is also relaxed to Levitus climatology as a result of the questionable accuracy of precipitation fields produced by the atmospheric reanalysis system.

The model is first spun up from zonally averaged WOA94 climatology for thirty

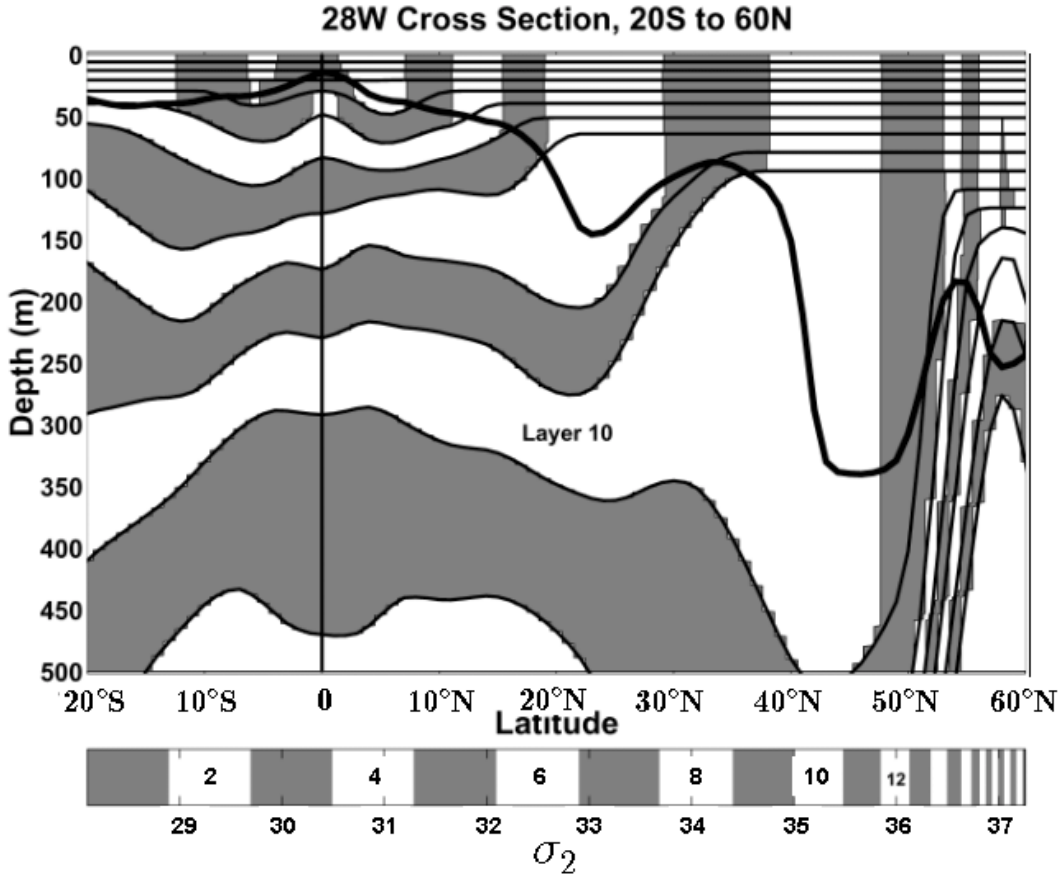

Figure 2. Cross-section of mean model density (σ_2) during winter (February) along 28°W from 20°S to 60°N. Mean model fields were calculated by initializing the model with the thirty-year spinup fields, integrating the model for ten years, then temporally averaging the ten February fields. The density range is divided into alternate white and gray bands, with each band centered on the reference density of a model layer. Even layer numbers from 2 through 12 are marked inside the shading bar. Alternating white and gray bands follow model layers in the isopycnic coordinate interior, but deviate from them in the non-isopycnic domain above. The thick line tracks the diagnosed mixed layer base.

years. The resulting fields are used as initial conditions for all subsequent simulations. These include a ten-year run, with fields saved monthly, to calculate the mean annual cycle of simulated fields. Properties of the hybrid vertical coordinate scheme are illustrated in the ten-year winter mean cross section of model density (σ_2) over the upper 800 m of the water column along 28°W (Figure 2). The isopycnic coordinates within the ocean interior smoothly transition to pressure coordinates near the surface. The KPP mixed layer base, diagnosed based on a minimum density jump criterion that takes into account the influence of variable salinity [*Kara et al.*, 2000b], is also illustrated.

The zonally integrated overturning streamfunction (Figure 3) shows that the model develops a MOC of about 16 Sv in the subtropical North Atlantic, 1-2 Sv larger than typical mean values estimated in earlier studies but within error

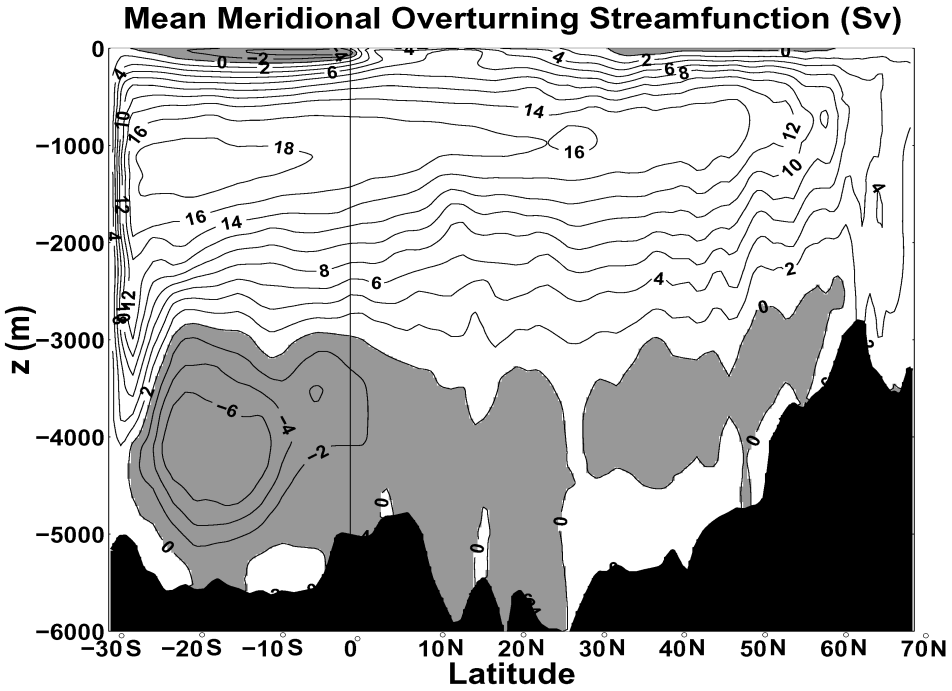

Figure 3. Streamfunction of the Meridional Overturning Circulation (Sv) averaged over the entire ten-year model simulation.

uncertainties. The overturning is largely imposed by the northern and southern boundary conditions. When the model is run without these relaxation boundary conditions, the MOC is very weak (<5 Sv). The southern boundary drives nearsurface inflow and deep outflow through geostrophic adjustment to the zonal density gradients forced by the relaxation. The southern boundary must account for all vertical advection and water mass transformation associated with the global overturning circulation that occurs throughout the Southern and Indo-Pacific Oceans. The northern boundary does not directly force large inflows and outflows, but may significantly influence deep water formation through the vertical density gradients set in the boundary. All but 4 Sv (25%) of deep water forms to the south of the boundary layer (Figure 3).

3.2. Float/drifter analysis in HYCOM

HYCOM is equipped with code to deploy and track synthetic floats and drifters during model run time using horizontal and temporal interpolation schemes adapted from algorithms originally developed for MICOM [*Garraffo et al*., 2001a*; Garraffo et al*., 2001b]. Float capabilities have been substantially extended in HYCOM. Floats released in MICOM always remain within the model layer in which they are released. As a result, they are isopycnic when released in the isopycnic coordinate interior [*e.g. Fratantoni,* 1996]. Isopycnic floats work well as long as diapycnal mixing is sufficiently weak. The MICOM floats act as surface drifters when released in the model mixed layer (layer 1), and these drifters have been successfully employed in Lagrangian prediction studies [*Garraffo et al.,* 2001a; 2001b]. However, neither isopycnic floats nor surface drifters are

adequate for studying pathways of thermohaline flows that are fundamentally non-isentropic. For this reason, HYCOM employs three-dimensional Lagrangian floats that are capable of tracking the flow of fluid parcels within a non-isentropic environment. The full three-dimensional velocity field of the model, including the diagnosed vertical velocity (Appendix 1), is horizontally interpolated to float locations using procedures described in Appendix 2 and then used to advect the floats by the Runga-Kutta temporal interpolation algorithm described in Appendix 3. For completeness, HYCOM also has options for isopycnic and isobaric (constant depth) floats, the latter capable of representing surface drifters when released in the top model layer.

To facilitate an understanding of float trajectories, dynamical and thermodynamical properties, including terms of the equation governing the vertical component of relative vorticity, are horizontally interpolated to the location of each float. Time series of float position and depth, along with the interpolated variables, are archived every two days for analysis. This study extends the Lagrangian model analysis of Blanke et al. [1999] who estimated vertically integrated transport streamfunction maps of different upper-limb water masses (surface, thermocline, etc.) approaching the equator from the south within a domain spanning 10 degrees north and south of the Equator. The present study extends that domain and explicitly resolves three-dimensional upper-limb transport pathways and the water mass transformations that occur along them.

It is important to point out that the three-dimensional Lagrangian floats will not exactly follow water parcels in the ocean because of errors in the interpolation of velocity components to float locations, and also because of the existence of unresolved (subgrid-scale) velocity fluctuations [*e.g. Haidvogel,* 1982]. However, *Harper* [2000] points out that errors in float paths are greatly reduced when the temporal resolution of the velocity fields used to advect model floats is high, as it is in the present study (Appendix 3). Errors resulting from subgrid-scale velocity fluctuations are not considered.

3.3. Vorticity balance analysis

Boudra and Chassignet [1988] studied the vorticity balance in a layer model with generalized vertical coordinates (a precursor of both MICOM and HYCOM) in simulations of the Agulhas retroflection. The vorticity balance, written in terms of the generalized vertical coordinate s, is obtained by taking the curl of the model momentum equation:

$$\begin{aligned}\frac{\partial \zeta_s}{\partial t} = & \underbrace{-\mathbf{v}\delta_s p \cdot \nabla_s\left(\frac{\zeta_s}{\delta_s p}\right)}_{\text{(A)}} \underbrace{-v\delta_s p \frac{\partial}{\partial y}\left(\frac{f}{\delta_s p}\right)}_{\text{(B)}} \underbrace{-\frac{(\zeta_s + f)}{\delta_s p}\nabla_s \cdot (\mathbf{v}\delta_s p)}_{\text{(C)}} \underbrace{-\mathbf{k}\cdot(\nabla_s \alpha \times \nabla_s p)}_{\text{(D)}} \\ & \underbrace{-\mathbf{k}\cdot\left[\nabla_s \times \left(\dot{s}\frac{\partial p}{\partial s}\right)\right]}_{\text{(E)}} \underbrace{+A_H \mathbf{k}\cdot\left[\nabla_s \times \left(\frac{\partial p}{\partial s}\right)^{-1}\nabla_s \cdot \left(\frac{\partial p}{\partial s}\nabla_s \mathbf{v}\right)\right]}_{\text{(F)}} \underbrace{-\mathbf{k}\cdot\nabla_s \times \alpha\frac{\partial \vec{\tau}}{\partial z}}_{\text{(G)}},\end{aligned} \tag{1}$$

(H)

where the subscript s indicates that the vertical coordinate is held constant during partial differentiation. Terms (B) through (D) contain pressure thickness expressions because the finite difference analog of the term $(\zeta + f)\mathbf{k} \times \mathbf{v}$ in the model momentum equation must be written as the finite difference analog of $[(\zeta + f)/\delta_s p]\mathbf{k} \times (\mathbf{v}\delta_s p)$ to conserve potential vorticity and potential enstrophy [*Bleck and Boudra,* 1981; *Boudra and Chassignet,* 1988; *Bleck,* 2002]. Terms (B) and (C) thus contain pressure thickness gradient terms in addition to terms that represent relative and planetary vorticity advection, respectively. The thickness gradient terms that arise from expanding (B) and (C) represent the change in vorticity within individual layers resulting from the flow component parallel to the layer thickness gradient vector in the presence of background planetary and relative vorticity, respectively. The terms thus represent an internal vortex stretching contribution arising from the formulation of the model in layer vertical coordinates.

For the purpose of the present study, we rewrite the vorticity balance as follows:

$$\underset{(A)}{\frac{\partial \zeta_s}{\partial t}} = \underbrace{-\mathbf{v}\delta_s p \cdot \frac{1}{\delta_s p}\nabla_s \zeta_s}_{(B)} \underbrace{-\beta v \delta_s p \frac{1}{\delta_s p}}_{(C)}$$

$$\underbrace{-\left[\mathbf{v}\delta_s p \zeta_s \cdot \nabla_s\left(\frac{1}{\delta_s p}\right) + v\delta_s p f \frac{\partial}{\partial y}\left(\frac{1}{\delta_s p}\right) + \frac{(\zeta_s + f)}{\delta_s p}\nabla_s \cdot (\mathbf{v}\delta_s p)\right]}_{(D)} \underbrace{-\mathbf{k} \cdot (\nabla_s \alpha \times \nabla_s p)}_{(E)} \qquad (2)$$

$$\underbrace{-\mathbf{k} \cdot \left[\nabla_s \times \left(\dot{s}\frac{\partial p}{\partial s}\right)\right]}_{(F)} + \underbrace{A_H \mathbf{k} \cdot \left[\nabla_s \times \left(\frac{\partial p}{\partial s}\right)^{-1} \nabla_s \cdot \left(\frac{\partial p}{\partial s}\nabla_s \mathbf{v}\right)\right]}_{(G)} \underbrace{-\mathbf{k} \cdot \nabla_s \times \alpha \frac{\partial \vec{\tau}}{\partial z}}_{(H)}.$$

The thickness gradient terms have been removed from (B) and (C), so they now represent the influence of relative and planetary vorticity advection, respectively, in the absence of layer thickness or bottom depth gradients. Terms (B) and (C) are written with pressure thickness in both the numerator and denominator because each pressure thickness expression is horizontally averaged over different grid points in the finite difference analog terms. The thickness gradient terms removed from (B) and (C) have been added to term (D), which now represents the total influence of vortex stretching caused by both local temporal changes in layer thickness and internal vortex stretching caused by flow within layers in the direction of layer thickness change. Of the remaining terms, (E) is the buoyancy torque, (F) represents the tilting/twisting of relative vorticity, (G) is the horizontal stress curl, and (H) is the vertical stress curl. Local change in relative vorticity results from the combined influence of terms (B) through (H). The change of relative vorticity along the pathway of a three-dimensional Lagrangian float results from the sum of terms (C) through (H).

During the model run, values of terms in (2) are accumulated over the time

intervals between float output times. At each output time, the terms (total vorticity change in s^{-1} since the previous output time) are interpolated to the float, stored for further analysis, and zeroed for the start of the next output cycle. Values of each term can then be directly compared to the actual change in relative vorticity that occurred over the same time interval.

4. EULERIAN ANALYSIS

4.1. Model fields

In HYCOM, upper layer water is confined above about 100 m while thermocline water extends from about 100 to 300m. Since virtually all floats that take the interior pathway originate in these upper and thermocline layers (Figure 1; Section 5), we focus on simulated fields within the upper 300 m. The zonally integrated overturning streamfunction field in Figure 3 validates this decision. South of the equator, we see that upper limb water flowing northward between the base of the Ekman layer and about 300 m, upwells at the equator. Between the equator and about 15°N, this upwelled water then flows northward within a thin surface boundary layer. *Roemmich* [1983] discussed this northward transport asymmetry about the equator (flow approaching from the south at depth and exiting to the north within the Ekman layer), which demonstrates the necessity for water mass modifications en route across the equator. This scenario is consistent with the dominant thermocline water pathway in Figure 1, which requires that most of this water upwell at the equator before moving north. Between 15 and 35°N, the northward flow downwells into the ocean interior in response to subtropical Ekman pumping. We demonstrate later that the water subducted in the interior subtropical gyre to a depth of about 100 m tends to move southward in accordance with layered thermocline theory, thereby guiding interior pathway fluid parcels into the North Equatorial Current (NEC) and the Caribbean Sea. This southward interior flow is masked in Figure 3 by the contribution of northward western boundary layer flow.

Given the importance of vertical advection to interior pathways, we present maps of winter and summer w (calculated as in Appendix 1) at depths of 30 m and 100 m in Figure 4. Upwelling and downwelling are a consequence of geostrophic and Ekman convergences and divergences, and large seasonal variations are seen throughout the tropical Atlantic in response to the seasonal migration of the Intertropical Convergence Zone (ITCZ). In particular strong upwelling and downwelling regions are present year round in the western boundary regions, and strong off-equatorial upwelling and downwelling bands present during summer are associated with the wind stress curl forcing of the tropical and equatorial gyres. Equatorial upwelling and subtropical downwelling are especially important for governing the pathways taken by fluid parcels because these processes act in regions where there are horizontal flow reversals with depth. Specifically, the eastward-flowing EUC underlies the westward-flowing South Equatorial Current (SEC) along the equator while northward Ekman wind drift overlies southward geostrophic flow in the southern portion of the northern hemisphere subtropical gyre.

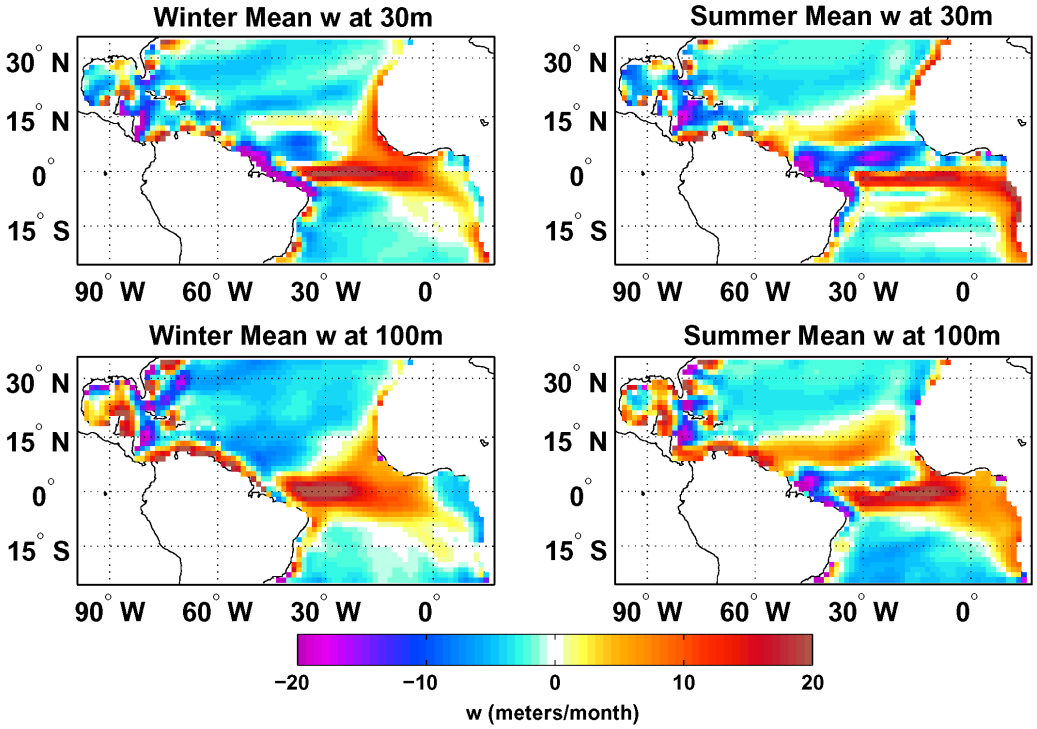

Figure 4. Winter (left) and summer (right) diagnosed vertical velocity w in meters per month at 30 m (top) and 100 m (bottom) estimated from (15) and averaged over all ten Februaries and Augusts, respectively.

The reversal of zonal equatorial flow with depth as represented by the model is illustrated by cross sections of u along the equator for winter and summer (Figure 5). The upward inclination toward the east of the model layers containing the EUC is greater in summer than in winter. For thermocline layer water that enters the EUC, a given water parcel will move upward by 30-50m as it travels eastward in winter and 60-80 in summer simply by following isopycnals. As demonstrated later, this initial upward motion brings water parcels close enough to the surface for Ekman divergence to upwell fluid across model interfaces and into the westward flowing SEC. This equatorial upwelling route is taken by a large fraction of upper-limb water that follows the interior pathway.

4.2. The seasonal internal energy storage and release mechanism

The seasonal internal energy storage and release mechanism for the tropical North Atlantic identified by *Philander and Pacanowski* [1986a; 1986b] is evident in the model fields. We illustrate this by integrating the meridional temperature flux times ρc_p eastward from the western boundary along each row of model grid points. Summer and winter maps of this field are shown in Figure 6, wherein the values along the eastern boundary represent the basin-wide meridional internal energy flux as a function of latitude. During winter, large northward internal energy flux exists across the entire basin at all latitudes. During summer, this northward flux is weaker across the entire basin between about 7 and 13°N.

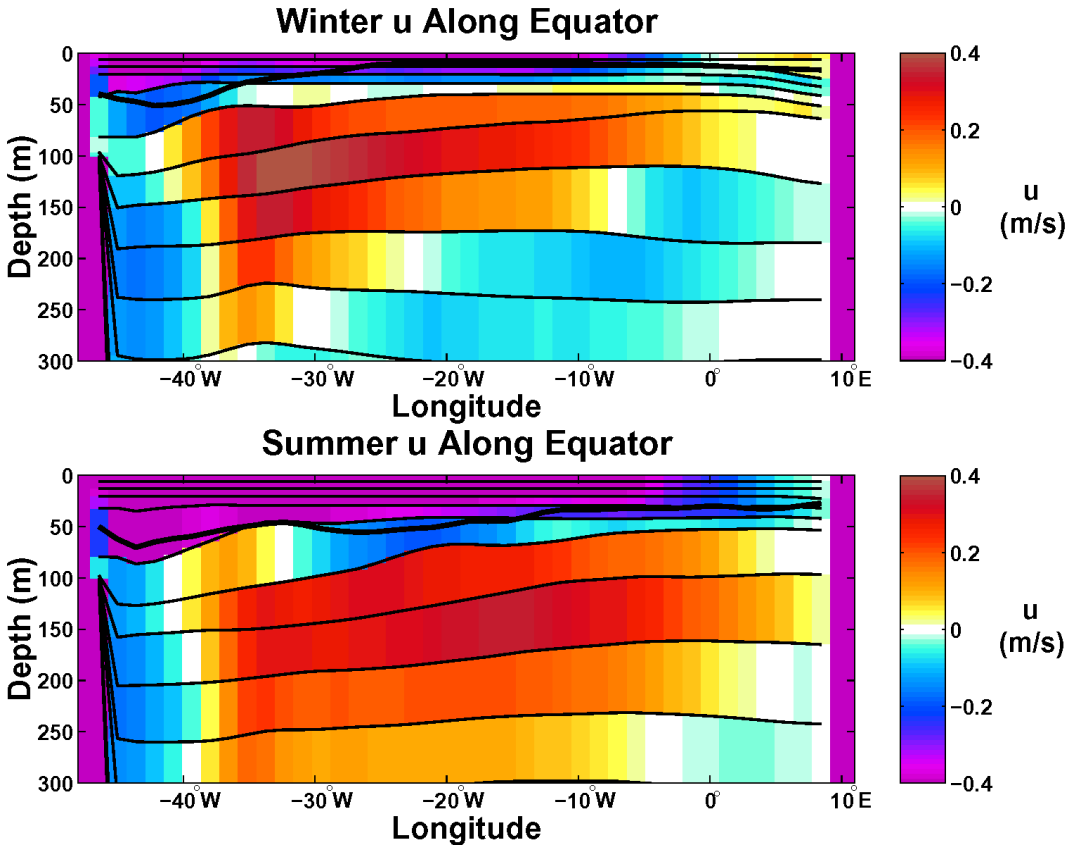

Figure 5. Zonal cross sections of winter (top) and summer (bottom) u (m s^{-1}) along the equator showing the zonal-depth structure of the EUC and the westward South Equatorial Current flow near the surface. These fields were averaged over all February and August maps, respectively, from the ten-year simulation.

Over the western two-thirds of the basin, it is either near zero or negative (southward). Internal energy therefore accumulates within the latitude band of the NECC during summer, primarily in the western two-thirds of the basin, and is released northward during the subsequent winter.

5. LAGRANGIAN ANALYSIS

5.1. Design of the southern hemisphere float release experiment

The primary goal of the float release experiment is to determine upper-limb fluid pathways from the southern hemisphere to the subtropical gyre of the northern hemisphere. Since our focus is on pathways extending into the North Atlantic interior, only the upper 300 m of the ocean is seeded with floats. Inspection of model horizontal velocity fields (not shown) demonstrates that a very large fraction of the MOC upper-limb fluid approaches the western boundary of the South Atlantic between 5°S and 14°S before turning north. This is validated by other model studies such as *Malanotte-Rizzoli et al.* [2001] and *Lazar et al.* [2002], which found that nearly all upper-limb flow approaching

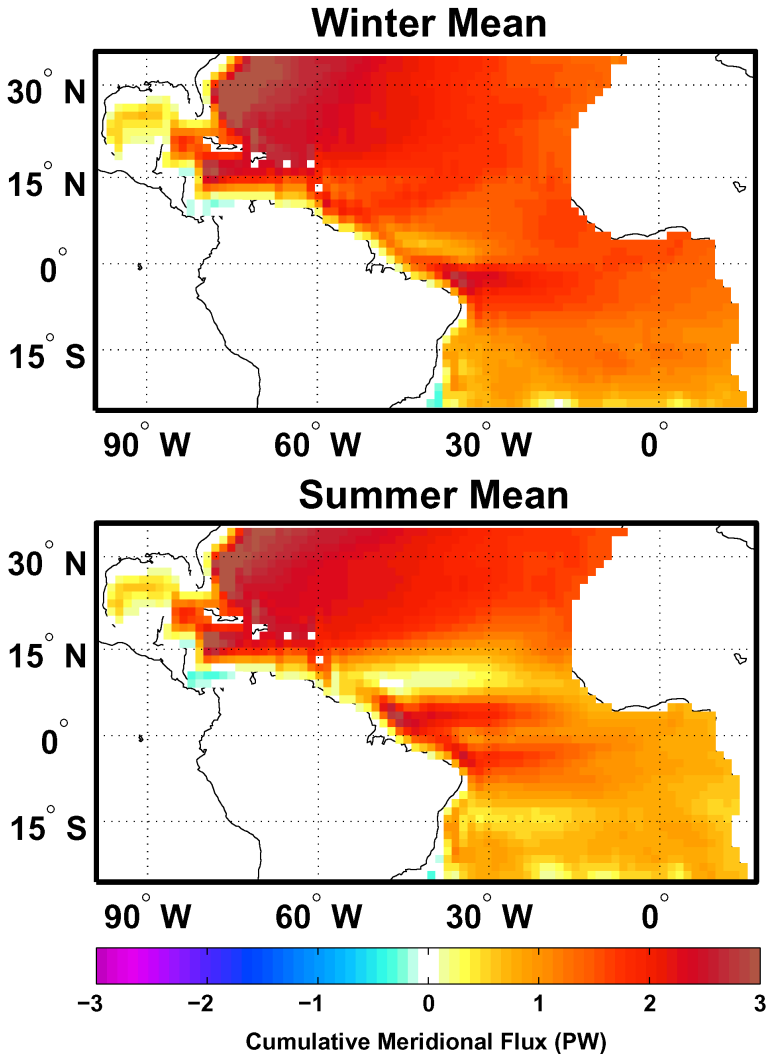

Figure 6. Cumulative meridional internal temperature flux times ρc_p integrated from the western boundary during winter (top) and summer (bottom). The value of this field along the eastern boundary is the net meridional internal energy flux (PW) as a function of latitude. The fields were averaged over ten Februaries and Augusts, respectively.

the equator did so in the western boundary. To capture the fluid that follows this general movement, individual floats are released at one-degree intervals in a box extending from 5 to 14°S and 28 to 32°W. Paths of surface and thermocline water are obtained by seeding floats at 25 m intervals between 25 m and 300 m. Such sets of releases are performed monthly over a full year for a total release of 7200 floats. The float release experiment is initialized with the thirty-year spinup fields and run for ten years, with all floats released during year one. All floats are advected five times per day while float positions and material properties are output for analysis every two days (Appendix 3). To aid in the interpretation of results, subsets of floats are selected based on where and when they were released and whether or not they entered one or more specified three-dimensional boxes within the model domain.

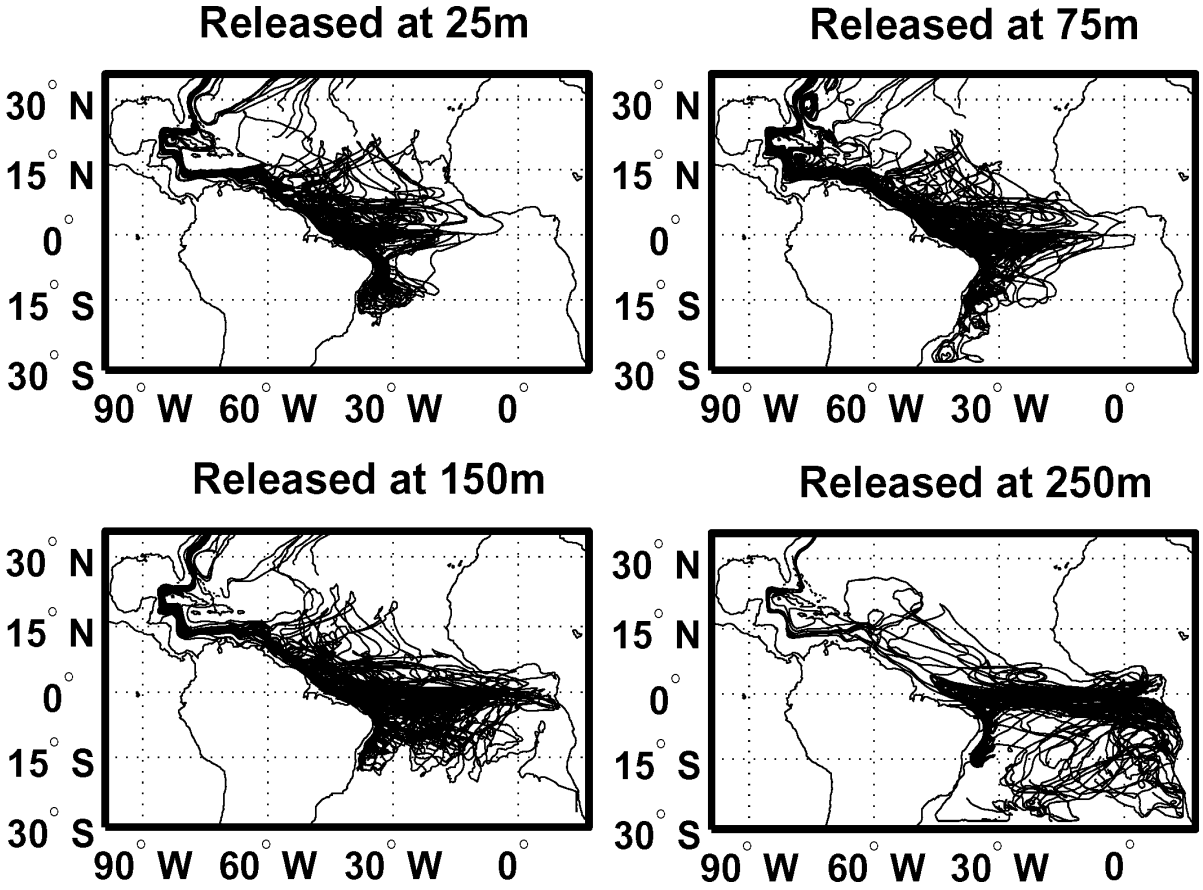

Figure 7. Path of floats released along 31°W during the entire year at 6, 8, 10, 12, and 14°S at four different depths (60 floats per plot).

5.2. Overview of simulated upper-limb pathways

A general overview of the float trajectories is provided by the pathline composites in Figure 7 for floats released at four different depths along 31°W at 6, 8, 10, 12, and 14°S. These composites demonstrate that upper-limb water parcels generally follow long, convoluted paths as they migrate northward. A large fraction of these floats spend part of their journey moving zonally along the equator, with the length of these equatorial excursions increasing with increasing release depth. A substantial fraction of the floats eventually populate the interior North Atlantic between 5 and 25°N. This number falls to zero for floats released at 300 m (not shown). Upper-limb fluid following interior pathways in the model is therefore composed almost entirely of surface and thermocline water, in agreement with Figure 1.

To begin validating the interior pathways hypothesis, we focus in on two subsets of the 7200 floats released. Both subsets contain floats that entered the North Atlantic interior via the NECC. The first subset includes floats that transited across the basin along the equator before returning westward and then entering the northern hemisphere. The second subset includes floats that took a more direct route northward past the equator. Three-dimensional pathlines for

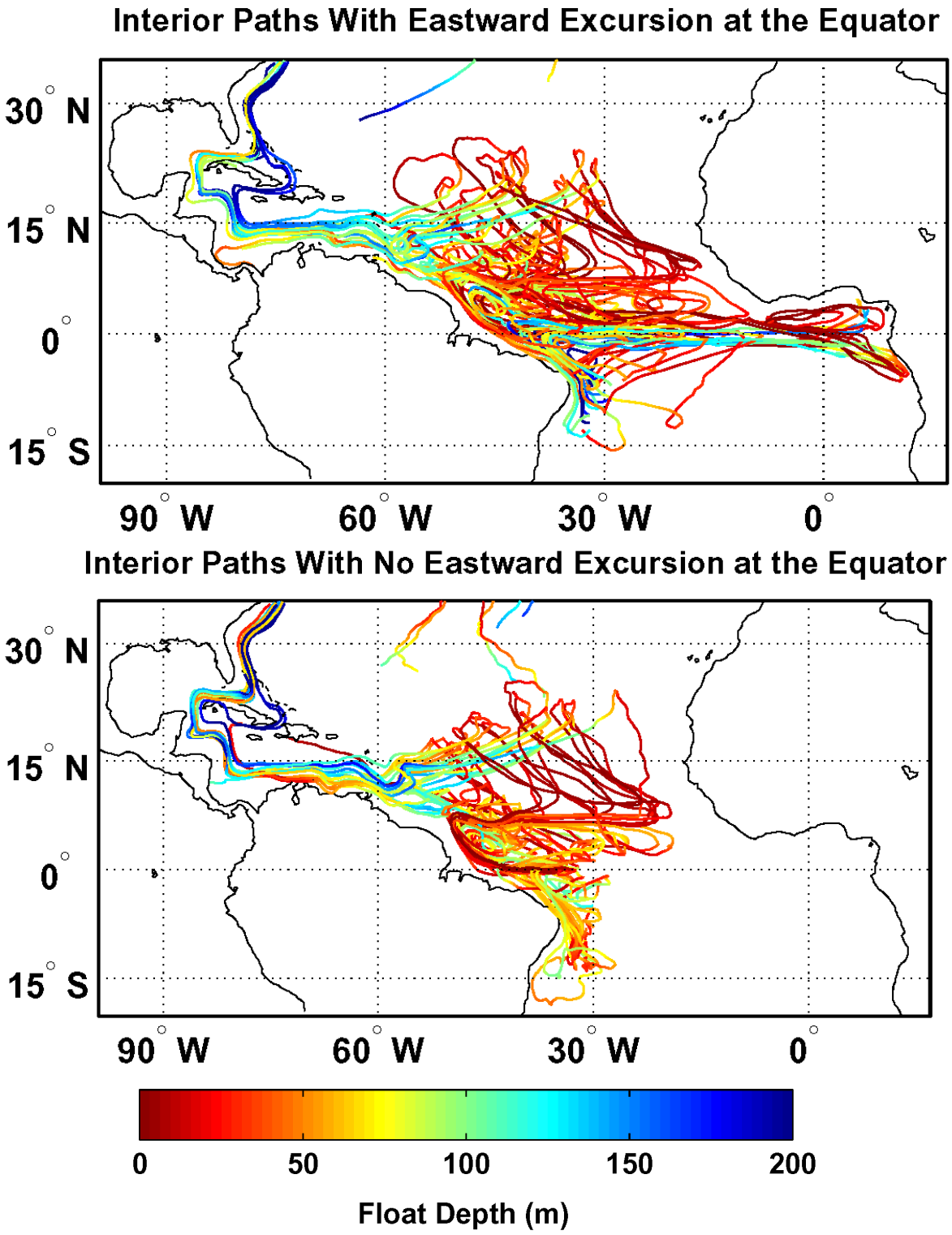

Figure 8. Float paths, color-coded to reveal depths along the paths. In both panels, a subset of floats released in the Southern Hemisphere box (5-14°S, 28-32°W) at one-degree intervals that followed interior pathways in the North Atlantic is displayed. In the upper (lower) panel, floats that did (did not) take a large eastward excursion at the Equator are selected.

both subsets are shown in Figure 8. These paths illustrate the importance of equatorial upwelling for bringing upper-limb water parcels (in particular lower surface layer and thermocline water) sufficiently close to the surface so that when they enter the ocean interior by way of the NECC (primarily in summer) they are advected northward in the Ekman layer in the following winter. The paths also illustrate some of the mechanistic details implied by the zonally integrated analyses of Roemmich [1983] and by Figure 3. Nearly all of the floats observed to transit across the basin in Figure 8 were released at depths of 100 m and greater, or primarily in the thermocline water. These floats had to spend more time at the equator undergoing water mass modifications as they moved upward into the SEC before heading farther north. Nearly all of the floats that did not transit across the basin were released at depths of 100 m and less, or primarily in the surface layer water. Although the time spent by these latter floats at the equator is relatively brief, equatorial upwelling is still a factor in moving them upward in the water column.

After moving upward into the SEC, these floats are advected to the western boundary and then northward. Nearly all of the floats in Figure 8 that reached the latitude of the NECC in the western boundary are located in the upper 40 m of the water column. They reach this latitude from late spring through fall when the wind-driven gyres are strong and the western boundary upper layer flow retroflects into the NECC. This seasonal dependence is illustrated by a special experiment where floats were released at 3 m depth at one-half degree longitude intervals along 4°N at the western boundary between 45 and 50.5°W. Two sets are considered, one released monthly from February through April and one released monthly from August through October (Figure 9). The large majority of floats released during the summer/fall interval when the ITCZ is positioned north of the equator and the tropical gyre is strong enter the interior in the NECC. In contrast, all floats released during the winter/spring interval when the ITCZ is positioned near the equator and the tropical gyre is weak proceed northward along the western boundary.

After moving eastward into the interior, most of the floats in Figure 8 then turn northward in the Ekman layer during the following winter as the easterly winds increase with the southward shift of the ITCZ. Floats that turn north must be sufficiently shallow to be advected by the northward Ekman wind drift. Floats released during summer/fall along the same 4°N line shown in Figure 9, but at depths of 50m and deeper (not shown) still enter the interior in the NECC, but circulate around the equatorial gyre instead of turning north during the following winter. Water parcels that take the interior pathway must therefore reach the NECC retroflection region in the upper 50 m of the water column during the late spring through fall time interval.

Eventually, floats following the interior pathway move sufficiently far north (>15°N, Figure 4) to be impacted by surface cooling and downward Ekman pumping. There they begin to subduct, moving slowly downward and towards the southwest. After spending an extended period of time in the interior during and after subduction (typically 2-4 yr as demonstrated later), the floats selected for display in Figure 8 enter the Caribbean at depths of around 100 m.

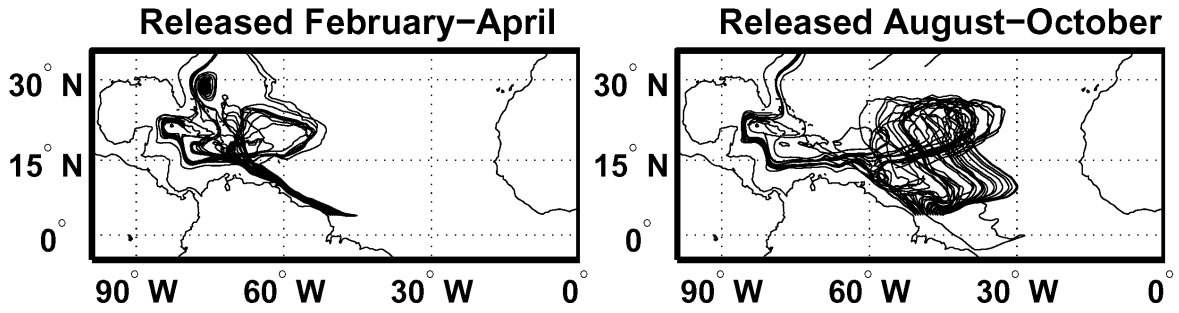

Figure 9. Paths of floats released between 50.5 and 45°W at 4°N at a depth of 3 m during winter and summer. Paths are shown over a time interval of four years.

None of these interior pathway floats follow a direct route to the subtropical North Atlantic along the western boundary, and all of the pathlines are non-isentropic. The paths of Figures 7 and 8 suggest a more complex scenario than the schematic of Figure 1. The pathways in Figure 1 assume that upper limb water will either follow the western boundary (either directly or within rings) or will follow one of two interior pathways: thermocline water upwelling at the equator and moving directly northward, or upper-layer water entering the NECC flow. The latter flow contains some thermocline water that upwelled and moved south from the equator before making a second attempt at crossing into the northern hemisphere. In the model (and likely in nature), equatorial upwelling allows some of the thermocline water at the equator to return directly to the western boundary and join the NECC interior pathway, which is not considered in Figure 1. Floats entering the NECC can also make one or more circuits of the equatorial gyre before either moving northward in the western boundary or taking the NECC interior pathway again and moving northward in the interior. Common to this complex set of pathways are the importance of depth during all phases of the annual cycle and the necessity for seasonally dependent water mass modifications en route.

5.3. Co-existence of the upper-limb MOC flow and subtropical cells

Another complexity not considered in Figure 1 is the North Atlantic subtropical cell, a focus of recent studies such as Malanotte-Rizzoli et al. [2001] and Lazar et al. [2002]. To visualize how the upper-limb MOC flow and subtropical cell coexist, two subsets of 25 floats that took interior pathways are selected; one set that entered the Caribbean and another that did not. Paths from each of these two subsets are plotted in both a meridional cross-section and a horizontal map (Figure 10). The subset that does not enter the Caribbean traces a subtropical overturning cell confined to the upper 120 m. The horizontal map shows that the return paths to the equator are convoluted, with many floats taking eastward excursions in the NECC, consistent with the results of Malanotte-Rizzoli et al. [2001] and Lazar et al. [2002]. Comparing horizontal maps of the two subsets, floats that subduct in the western part of the basin are more likely to enter the Caribbean than floats that subduct in the eastern part. Other factors such as wind stress forcing [Inui et al., 2002] and seasonal variability also play a role.

There is also the question of the existence of the North Atlantic subtropical cell. This cell clearly exists in this study and in other low-resolution model studies [*Malanotte-Rizzoli et al.*, 2001; *Lazar et al.*, 2002]. In contrast, nearly all of the particle-following floats released in the North Atlantic subtropical subduction zone in the high-resolution model study of *Harper* [2000] entered the Caribbean versus advecting to the equator. Further analysis of the interaction between the MOC and the North Atlantic subtropical cell will therefore be deferred to future high-resolution simulations.

5.4. Importance of using particle-following floats to track upper-limb pathways

Neither isopycnic floats nor surface drifters can reproduce complete upper-limb interior pathways such as those presented in Figure 8. Upper-limb pathways revealed by both isopycnic and three-dimensional Lagrangian floats are compared by releasing isopycnic floats in the southern hemisphere release box at a depth of 175 m during four seasons: February, May, August, and November (Figure 11). The resulting 200 isopycnic floats are compared to the 200 three-dimensional Lagrangian floats released at the same depth and times as part of the full southern hemisphere release experiment. A large fraction of the Lagrangian floats enter the northern hemisphere, many following interior paths.

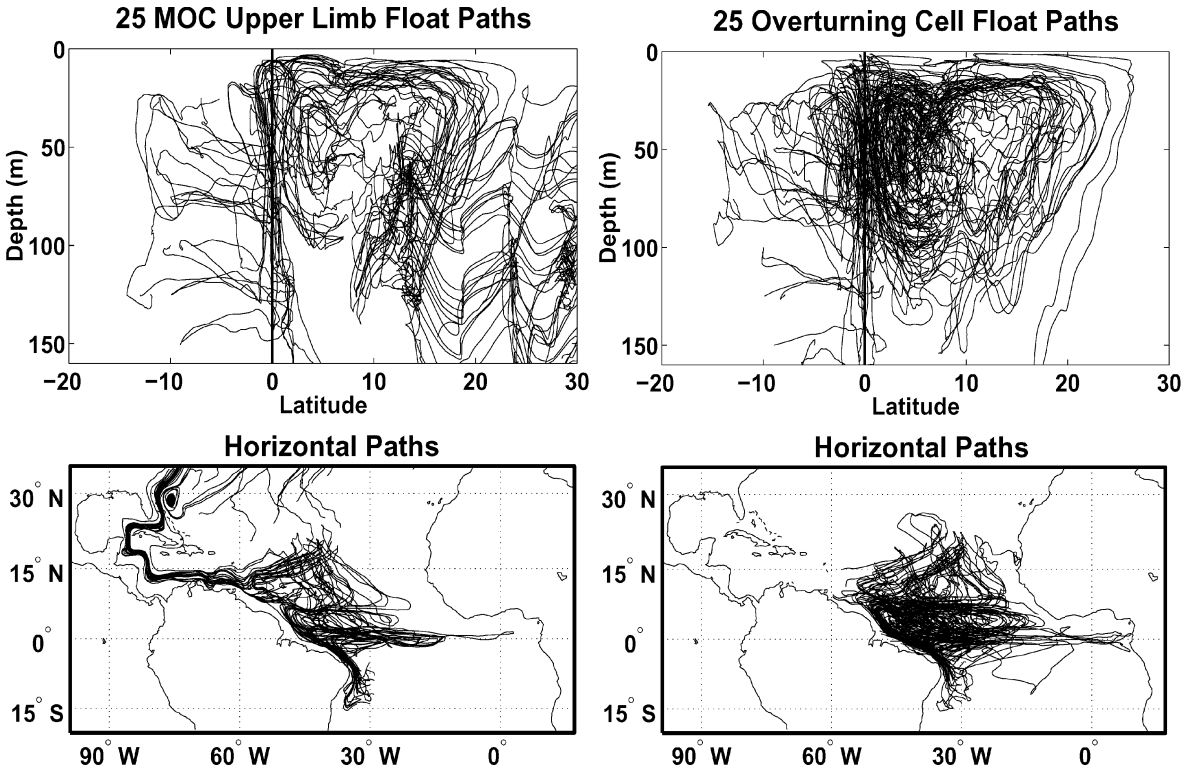

Figure 10. Paths in meridional-depth space (top), and in horizontal maps (bottom), of 25 floats that followed the interior pathway. Floats that entered the Caribbean as part of the MOC are shown in the left panels while floats that returned to the equatorial region as part of the North Atlantic subtropical overturning cell are shown in the right panels.

In contrast, the isopycnic floats remain in the same model layer and cannot upwell into the westward flowing SEC at the equator. As a result, these floats remain permanently confined near the equator or along the eastern boundary region off the African coast. Isopycnic floats released in the southern hemisphere thermocline water cannot reproduce the fluid pathways into the northern hemisphere. This result also supports the necessity of equatorial upwelling for thermocline water to eventually follow an interior pathway (Figure 1).

Upper-limb pathways revealed by both surface drifters and three-dimensional Lagrangian floats are compared by releasing both types of floats at a depth of 3 m at 2-degree latitude intervals along a meridional line located at 30°W (Figure 11). Over a three-year time interval, the Lagrangian floats are observed to deepen north of about 15°N and to begin their southwestward journey toward either the Caribbean Sea or the equator. In contrast to this, all of the surface drifters continue northward in the Ekman layer until they are trapped in the subtropical convergence zone. For floats to properly track fluid pathways in the subtropical North Atlantic, they must deepen in response to Ekman pumping.

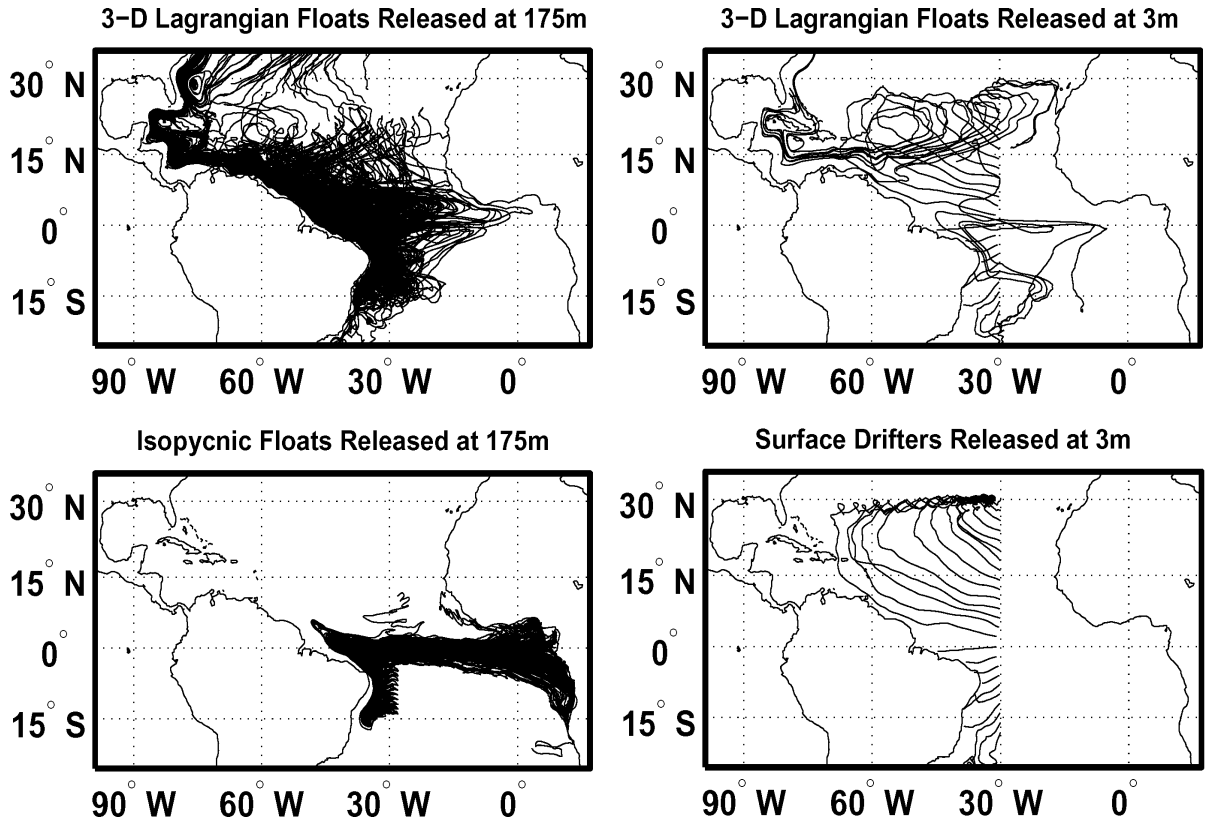

Figure 11. Illustration of the strong dependence of results on the type of float used. Paths of Lagrangian floats (top left) and isopycnic floats (bottom left) released in the southern hemisphere release box (5-14°S, 28-32°W) at a depth of 175 m on 1 February, 1 May, 1 August, and 1 November (a total of 200 floats in each panel). Also shown are paths of Lagrangian floats (top right) and surface drifters (bottom right) released at a depth of 3 m along 30°W at two-degree latitude intervals.

Although the limitations of both isopycnic floats and surface drifters are evident in Figure 11, we do not mean to imply that they cannot be used to study many aspects of flow pathways in the tropical Atlantic Ocean or in other regions. For example, the use of isopycnic model floats to delineate the return flow of subtropical cells to the equator [Malanotte-Rizzoli et al., 2000; Lazar et al., 2002] is reasonable because the flow along these path segments is only weakly non-isentropic. Neutrally buoyant floats have been successfully used in a wide range of observational studies. Surface drifters can provide useful information over time intervals sufficiently short so that subduction is not important, or so that they do not become trapped in convergence zones. However, a holistic picture of pathways taken by a fundamentally non-isentropic flow such as the upper limb of the MOC can only be delineated using three-dimensional Lagrangian floats.

5.5. Float census

Of the 7200 floats that were released in the southern hemisphere, only 2823 penetrated north of 8°N during the ten-year simulation. A total of 2646 of the floats eventually entered the Caribbean as part of the MOC upper-limb flow. Of the floats entering the Caribbean, a total of 272 (10.3%) take an interior pathway by flowing directly northward from the equator. A total of 361 floats (13.6%) take an interior pathway by flowing eastward within the NECC from the western boundary region. The remaining 2013 floats (76.1%) flow into the Caribbean without taking one of the interior pathways. Of these, 651 flowed directly along the western boundary from the southern hemisphere into the Caribbean without taking an eastward excursion along the equator.

To assess the relative importance of the North Atlantic subtropical cell, there are 418 floats that took one of the interior pathways but never entered the Caribbean Sea. All but a small number of these floats returned to the equator after subducting in the subtropical North Atlantic. Although a larger number of subducted floats entered the Caribbean than did not, we point out that some of the floats entering the Caribbean actually returned to the equator at least once as part of the subtropical cell. Consequently, the importance of the subtropical cell in the model is larger than indicated by the numbers given above. Moreover, since subduction releases energy to the atmosphere, subducted floats returning to the equator via the subtropical cell contribute to the upper limb northward heat flux whether or not they end up in the Caribbean or points farther north.

With nearly 1/4 of upper limb floats that entered the Caribbean having taken an interior pathway during part of their existence, these pathways are clearly important in the model simulation. This percentage is in close agreement with the 25% estimate of *Schott et al.* [1998]. While we again caution against using low-resolution results to update quantitative estimates, the present results do provide a qualitative verification on the interior pathway importance.

6. CASE STUDIES AND MECHANISMS

So far the path compilations show the upper limb pathways to be fully three-dimensional and seasonally dependent. Equatorial upwelling, water mass

modifications, and eventual subduction are attributes of all model floats that take interior pathways. We now turn our attention to physical mechanisms that permit the floats to navigate across the equator and between the various gyres. We do this through case studies, focusing in on six individual floats whose paths are illustrated in Figure 12. We compare five floats that took interior pathways to one that did not. Floats 1 and 2 correspond to the two cases highlighted in Figure 8; i.e., floats that follow the interior pathway via the NECC and enter the

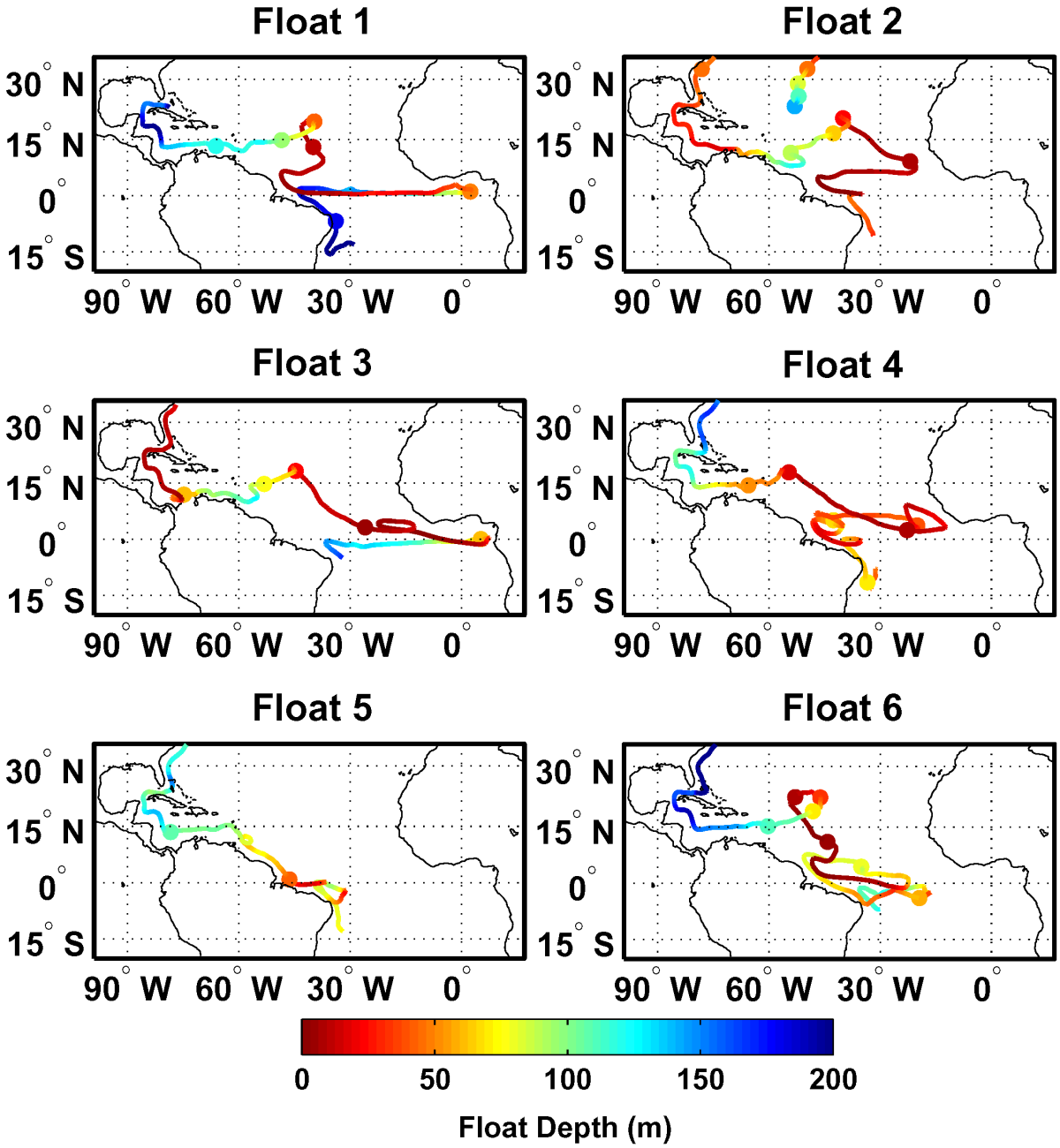

Figure 12. Paths of six floats color-coded to reveal the depth. Dots are plotted on 1 January of each year reveal the temporal progression along the paths.

Caribbean, but with one first transiting along the equator and the other not. Float 3 also transits along the equator across the basin and upwells into the SEC, but it moves northward into the interior long before reaching the western boundary. Float 4 transits eastward within the NECC and completes a circuit around the clockwise equatorial gyre before entering the North Atlantic subtropical gyre via the ocean interior. It does not initially turn northward because it is at a depth of 40-50 m, or below the northward Ekman wind drift. It crosses its original eastward path into the interior at a time of year when the NECC (and hence the cyclonic tropical gyre) is not strongly developed. Float 5 directly follows the western boundary into the Caribbean. Float 6 follows the interior pathway via the NECC. However, this float shows a more convoluted path, including one complete cycle around the equatorial gyre. Floats 1-5 are selected to provide relatively simple examples of float behaviors. Float 6 is representative of the more typical float that requires multiple attempts at entering the North Atlantic subtropical gyre before actually doing so. This complexity must eventually be taken into account in flow diagrams such as Figure 1. Common to the five floats in Figure 12 that take interior pathways is that they spend a long time in the interior, typically 2-4 yr.

Along each of these float paths we sample horizontal position, depth, model layer number, temperature, salinity, density (σ_2), relative vorticity, and the material derivative of relative vorticity. We also sample the eight terms that comprise the water parcel's relative vorticity balance, with terms labeled according to the letters designated in (2). These time series are shown in Figure 13a for the first six years of the Float 1 trajectory. We emphasize Float 1 in the time series analysis since it represents the principal attributes of the interior pathway hypothesis and because the processes acting on similar path segments of other floats are very similar to those acting on Float 1. The time history in Figure 13a includes pivotal segments of the float's trek to the Caribbean. These segments are: (1) retroflection into the EUC, (2) eastward flow within the EUC, (3) retroflection into the NECC, (4) northward flow in the interior Ekman wind drift, and (5) post-subduction southwestward flow into the NEC. Vertical shading bars highlight these five time intervals in Figure 13a, and time series for all segments except (4) are presented in expanded detail in Figures 13b-e because it is difficult to see important aspects of the vorticity balance in Figure 13a. Figure 13f adds further insight by focusing on that part of the history of Float 5 where it flows directly along the western boundary without retroflecting into the NECC. Errors in the estimation of vorticity balance terms would be a significant issue if we were trying to perform a Lagrangian vorticity budget analysis and prognostically forecast vorticity evolution along pathways. In the present study, however, we analyze the Eulerian vorticity budget along relatively short path segments. At the beginning of each path segment, the fluid parcel has undergone such large prior modifications from processes such as equatorial upwelling and subtropical subduction that it can essentially be considered a new parcel with new initial conditions. In these path segments, we are able to clearly identify the dominant terms in the balance that act to control the motion of fluid parcels.

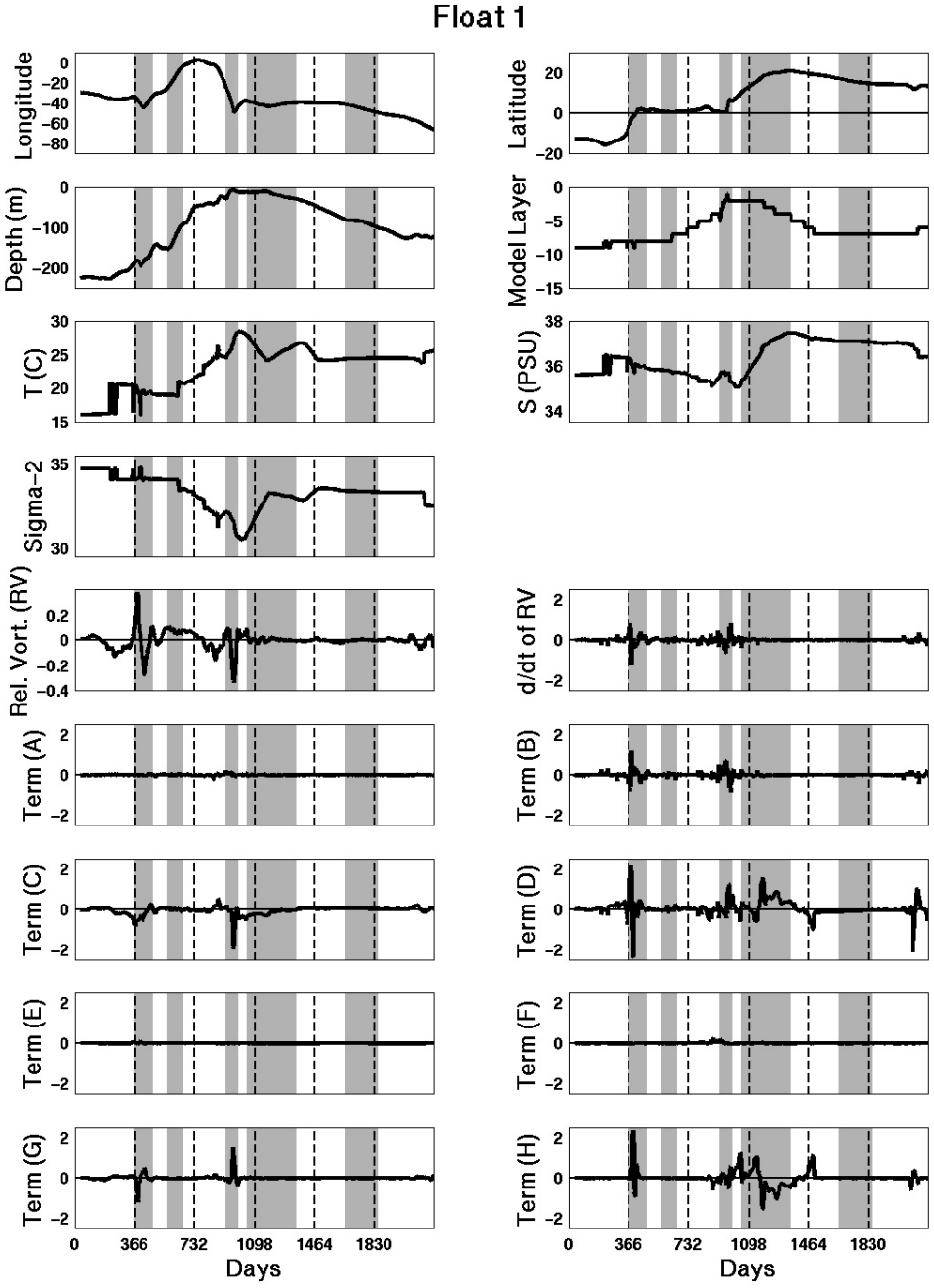

Figure 13a. Time series of several variables interpolated to the position of float 1 during the first six years of its existence The top seven panels contain position and thermodynamical variables. The bottom ten panels contain the vorticity analysis, specifically relative vorticity (RV), the material derivative of observed RV, and terms (A) through (H) of the relative vorticity equation (2). Shading indicates time intervals emphasized in the text. Vertical dashed lines mark one-year intervals (the model year is 366 days long).

6.1. Float 1 approaches the equator and retroflects into the EUC

We begin our discussion of mechanisms with the time interval (days 360-480) when Float 1 approaches the equator from the south and turns east to begin its transit across the basin. The top two panels of Figure 13b (relative to the top left panel of Figure 12) show that the approach, including an overshoot of the equator, occurs through day 420 as the float moves northwestward along the western boundary. During this time, the depth is at first relatively constant, it deepens slightly as the float approaches the equator, and it then shoals steadily after the equator is reached. Temperature and salinity both covary to keep the density relatively constant. The float is located in model layer 8 except for a brief interval near day 400 when it moves into model layer 9. This produces an abrupt change in float thermodynamical properties that may be viewed as a truncation error resulting from the discrete model layers.

During the initial stage of the approach when the float is moving to the northwest along the western boundary the relative vorticity is positive and increasing despite the planetary vorticity tendency (C) acting to decrease it. The controlling term is the stretching term (D) as the thermocline slope decreases along the western boundary toward the equator to ensure a continuous slope across the equator. Positive relative vorticity starts to decrease around day 380 assisted by horizontal stress torque (G). At about 2.5°S the stretching term reverses and the vertical stress torque (H) increases to compensate for this. This corresponds to entry into the equatorial visco-inertial boundary layer [Charney and Spiegel, 1971], where the thermocline deepens and increased dissipation (via vertical friction) is necessary to constrain the relative vorticity. Thereafter, relative vorticity decreases primarily by planetary vorticity advection as the float overshoots the equator to about 2°N as it retroflects into the EUC. Once heading eastward and eventually back toward the equator the relative vorticity is controlled by planetary vorticity advection plus vortex stretching, the latter partly compensated by relative vorticity advection.

The equatorial visco-inertial boundary layer region of the model is located within about 3 degrees of the equator. As in nature, it arises so that meridional derivatives may be continuous across the equator. Since planetary vorticity advection acts to decrease (increase) the relative vorticity of fluid approaching from the south (north) a cusp in zonal velocity would form on the equator were it not for frictional smoothing. For this particular float, vertical friction torque is the primary smoothing agent with horizontal friction of secondary importance.

In summary, the dynamical approach of the float to the equator is in the form of a modified inertial jet adhering to the western boundary. When the jet encounters the equatorial boundary layer its dynamics are altered such that vertical friction plays a larger role. Kinematically, we see how the float is steered by the flow field. From day 360-385, the float hugs the western boundary maintaining positive relative vorticity. It is freed from this constraint around day 385 by entering the equatorial visco-inertial boundary layer, which causes relative vorticity to become negative. Upon overshooting the equator, the accumulated negative relative vorticity is sufficiently large for the float to retroflect eastward and equatorward.

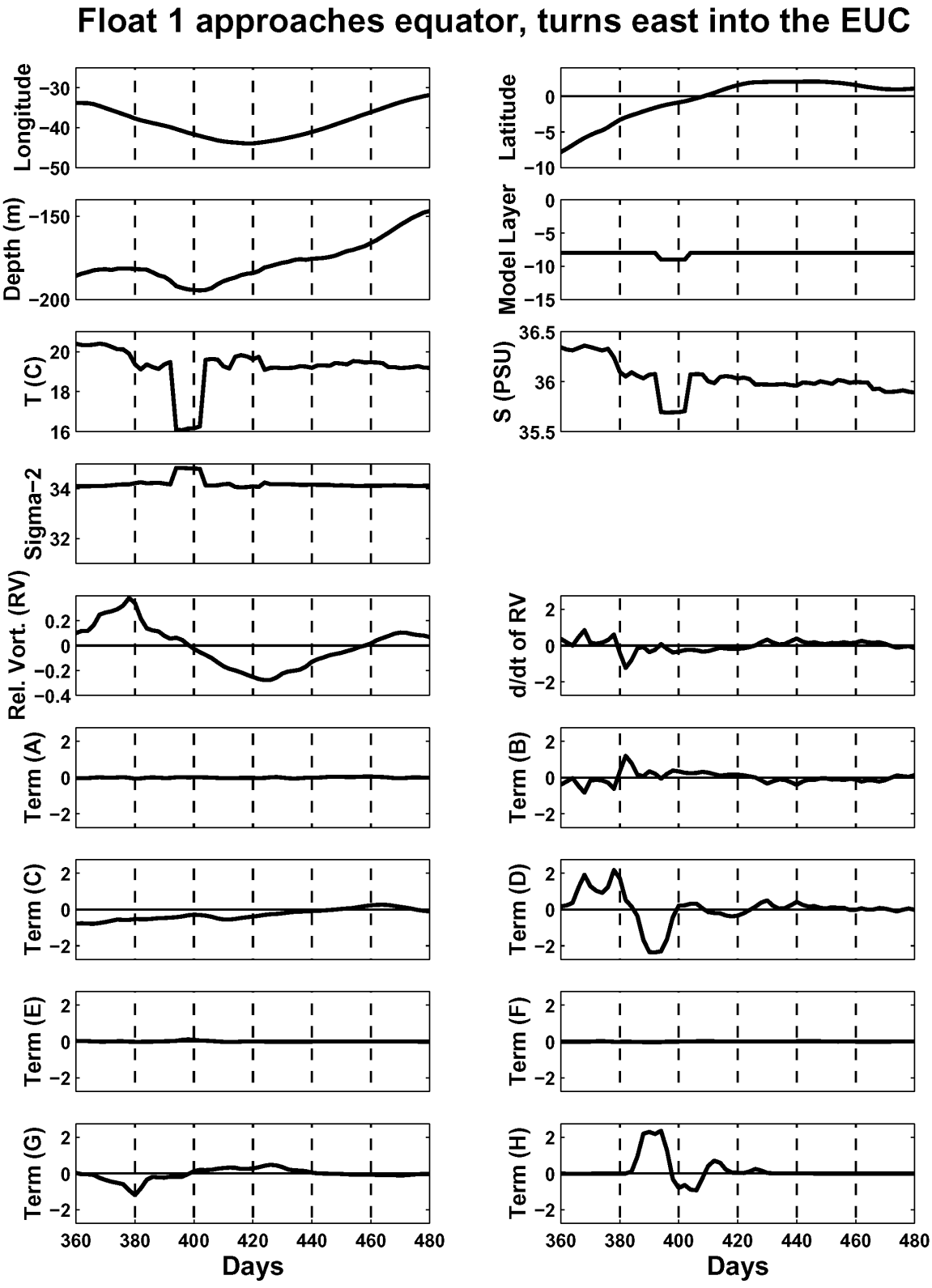

Figure 13b. Same as Figure 13a, but for a short segment along the path of float 1 when it advects northward along the western boundary to the Equator and retroflects eastward into the EUC.

6.2. Float 1 transits across the basin along the equator

The next segment of the Float 1 journey is provided by Figure 13c, which highlights the eastward movement across the basin within the EUC over days 560-660. During this time, after the float has adjusted to its overshoot of the equator and the balance terms show minimum variability, the float remains slightly north of the equator and steadily rises in depth by about 90 m. Relative vorticity remains positive (the float is in the cyclonic shear region of the EUC), but displays noticeable oscillations. The lead terms in the vorticity balance include non-linear advection (B), vortex stretching (D), planetary advection (C), and local rate of change (A). Terms (C) and (A) tend to covary at about 20-day time scale consistent with tropical instability waves near the equator [e.g., Weisberg and Weingartner, 1988; Weisberg and Qiao, 2000]. Terms (B) and (D) also tend to covary suggesting that vortex stretching is accommodated by an advective rate of change in relative vorticity along the float path.

Eventually, the float is close enough to the surface to flow westward within the SEC. This reversal occurs near day 750 in Figure 13a. Prior to and subsequently, the float upwells steadily through the water column undergoing significant changes in T, S, and σ_2 as the float continues to cross through several model layers. So long as the latitude changes are small, however, there are no major changes in relative vorticity and hence no need for large terms in the balance tendencies. During this stage the float (or simulated water parcel) is increasing its internal energy via surface heat flux and hence increasing its potential for contributing toward the net northward internal energy flux by the MOC. By the latter stages of this westward transit (illustrated in Figure 13d) the water properties associated with Float 1 are entirely different from the properties when it was initially released.

6.3. Float 1 departs from the equator and enters the NECC.

The Float 1 movement westward is relatively uneventful through around day 950 (Figure 13d). It then approaches the western boundary and turns more rapidly northward along this boundary around day 960. This is followed by eastward retroflection into the NECC around day 970. Western boundary effects first become evident after day 945 when relative vorticity begins to decrease. It reaches its largest negative values during retroflection.

The relative vorticity decrease around day 945 is initiated by both the vortex stretching term (D) and the horizontal stress term (G), the former because the thermocline slopes up into the western boundary in the northern hemisphere to accommodate a northward flow. As the northward turn takes effect, planetary vorticity advection then becomes the leading term in generating negative relative vorticity. Coincident with this, however, we see an increase in horizontal frictional torque, which tends to offset planetary vorticity advection, thereby limiting the decrease in relative vorticity. The counteraction of these two terms indicates that horizontal frictional boundary layer dynamics [*Munk,* 1950] play a significant role in the western boundary of the equatorial gyre. This is different from the modified inertial boundary layer behavior described by Fig 13b when the float first approached the western boundary from the southern hemisphere at

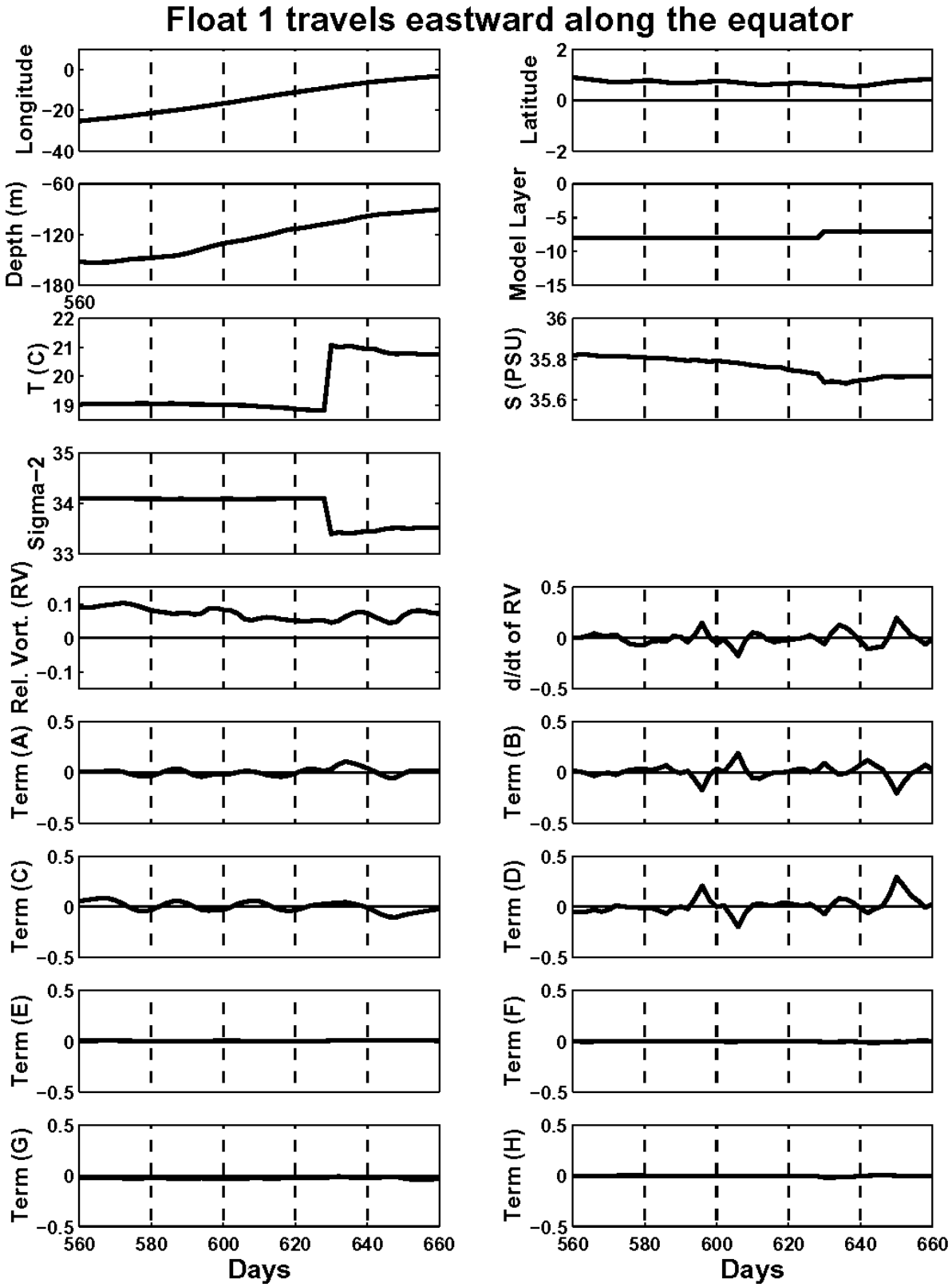

Figure 13c. Same as Figure 13a, but for a short segment along the path of float 1 when it advects eastward along the Equator within the EUC.

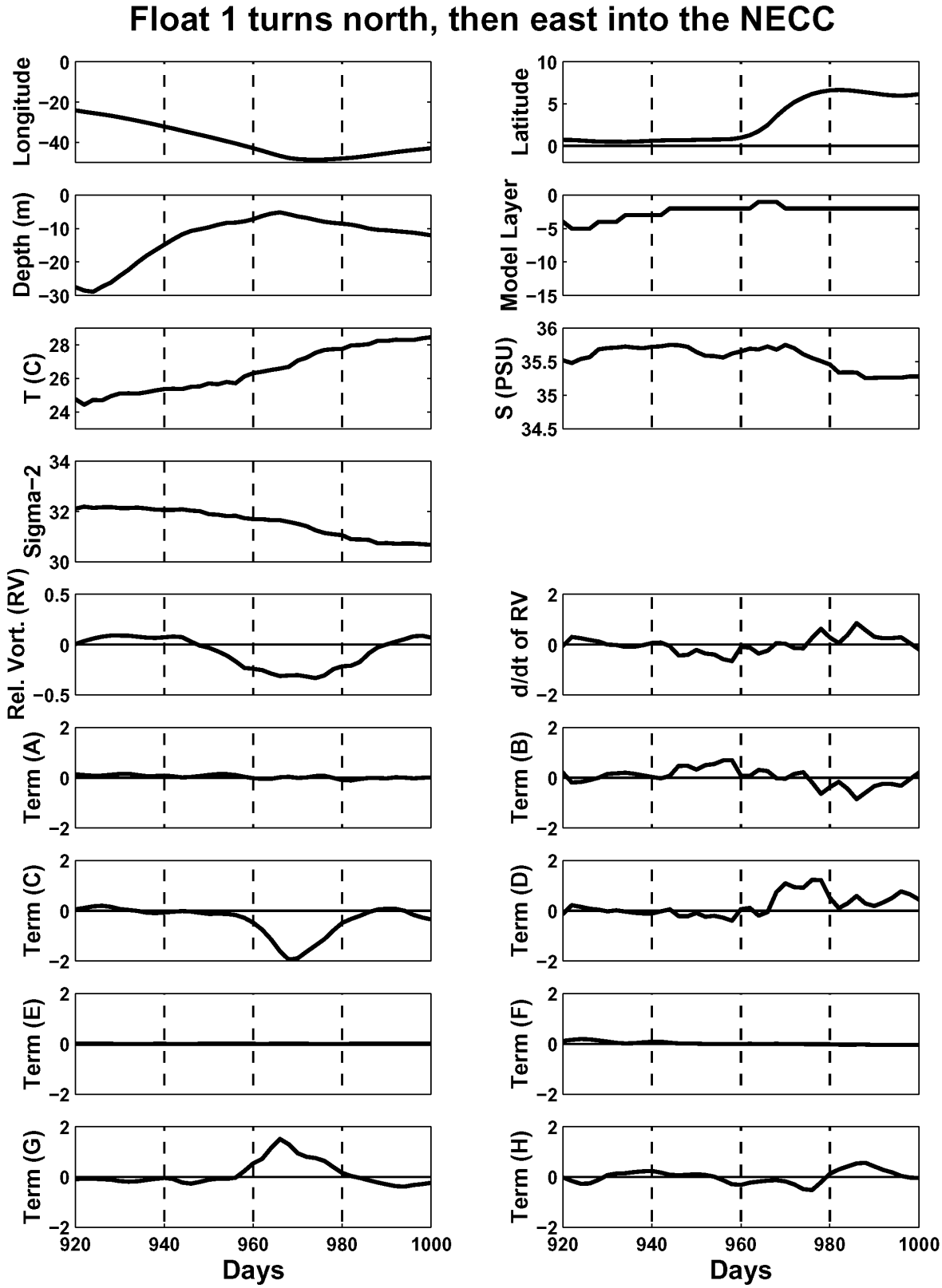

Figure 13d. Same as Figure 13a, but for a short segment along the path of float 1 when it retroflects into the NECC from the western boundary.

its initial depth deeper in the thermocline. There, positive relative vorticity tendency by the stretching term worked to keep the float attached to the western boundary prior to entering the equatorial visco-inertial boundary layer where the sign of the stretching term reversed. We also note that the dominance of frictional boundary layer dynamics in the model results in part from the low resolution. In high resolution models, as in nature, this boundary layer is more inertial, to the point of shedding NBC rings [*Barnier et al.*, 2001].

Once retroflection begins and the float moves toward the north and then the east, the stretching term becomes large and positive as the float moves away from the western boundary and into the region of the NECC ridge where the surface layer thickens. Movement away from the western boundary (where Munk layer dynamics prevail) coincides with a decrease in the horizontal stress torque so it is the effect of the stretching that brings the relative vorticity back to nominal values, assisted to a lesser degree by vertical friction torque. This tendency by stretching relaxes when the float attains its new quasi-equilibrium latitude at about 6°N where the float is readjusted and able to proceed eastward in the NECC. It cannot proceed farther north until something else happens. That something else is a vertical friction torque considered next.

6.4. Float 1 moves northward in the interior North Atlantic.

The new ingredient that begins to take effect shortly after retroflection into the NECC is a positive vertical stress torque (by wind stress curl). This effect is observed in Figure 13a approximately between days 1020 and 1160, the time interval during which the float travels northward from the NECC to the southern subtropical gyre. With Float 1 residing in the surface Ekman layer, the vertical friction torque by positive wind stress curl over the tropical gyre is balanced primarily by planetary vorticity advection as the float moves farther northward in the Ekman layer. Around day 1160, the sign of the wind stress curl reverses upon entering the subtropical gyre. There, vortex stretching compensates for vertical stress torque as the float deepens. During this time, temperature oscillates at the annual cycle and Float 1 begins to subduct. Eventually, when it is deep enough and below the surface Ekman layer, the float begins to return back toward the south and then southwest. For the initial stages of subduction, as the depth increases and the model layer number containing the float monotonically increases, the vorticity balance remains primarily between vertical friction torque and vortex stretching. The strong tendency of vortex stretching to balance vertical stress torque from the time the float leaves the NECC to the time it subducts in the subtropical gyre demonstrates the leading order importance of Ekman dynamics on the interior transport mode.

6.5. Float 1 moves southwestward after subduction in the subtropical gyre.

We begin after the float is fully subducted and continuing to slowly deepen. During this time interval from day 1650 to day 1850, the float remains in model layer 7 (Figure 13e). Frictional torques are now small since the float is below the Ekman layer and away from other boundaries. Hence, the vorticity balance is primarily between the vortex stretching and the planetary vorticity advection

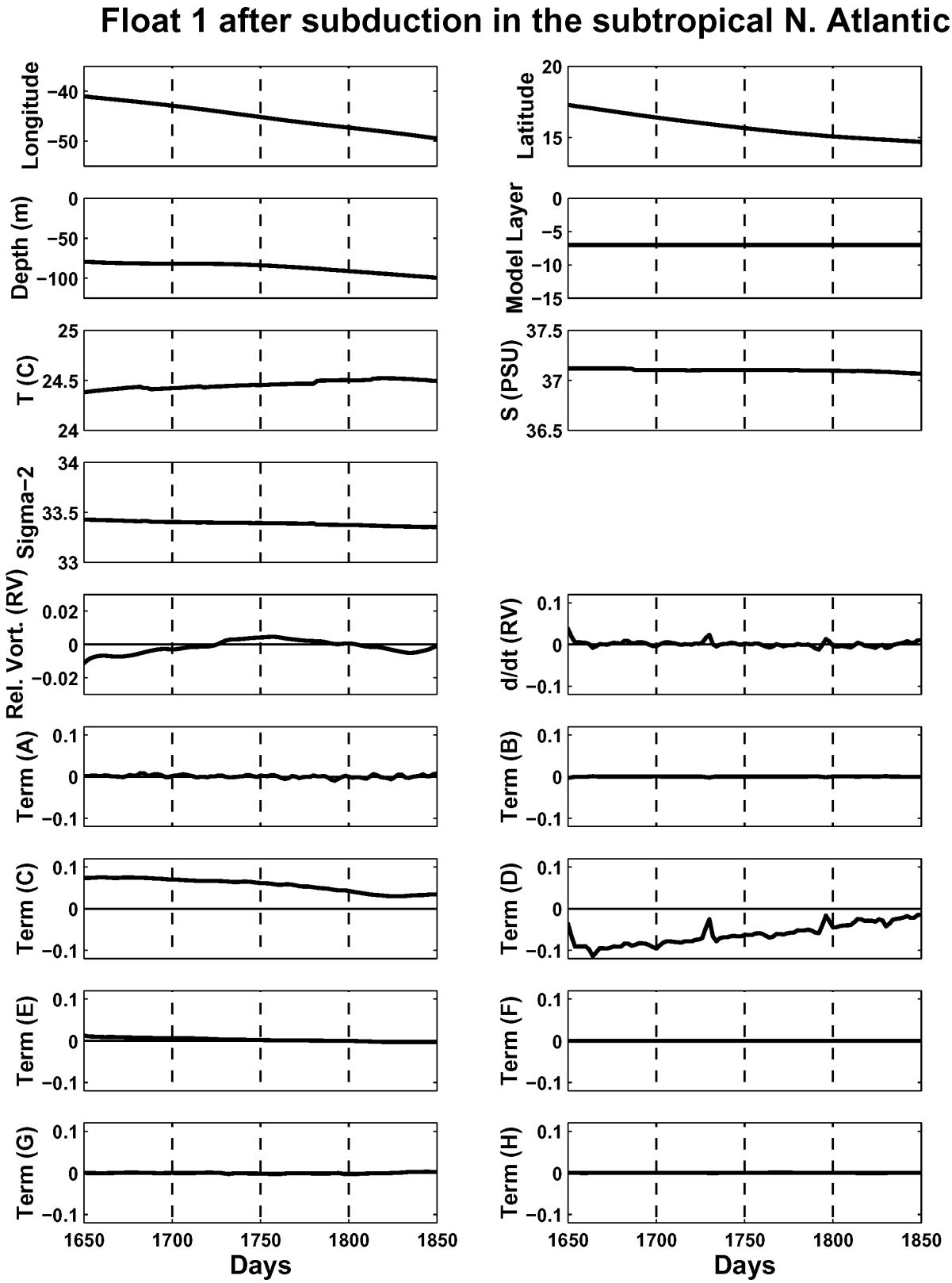

Figure 13e. Same as Figure 13a, but for a short segment along the path of float 1 after it subducts in the subtropical North Atlantic.

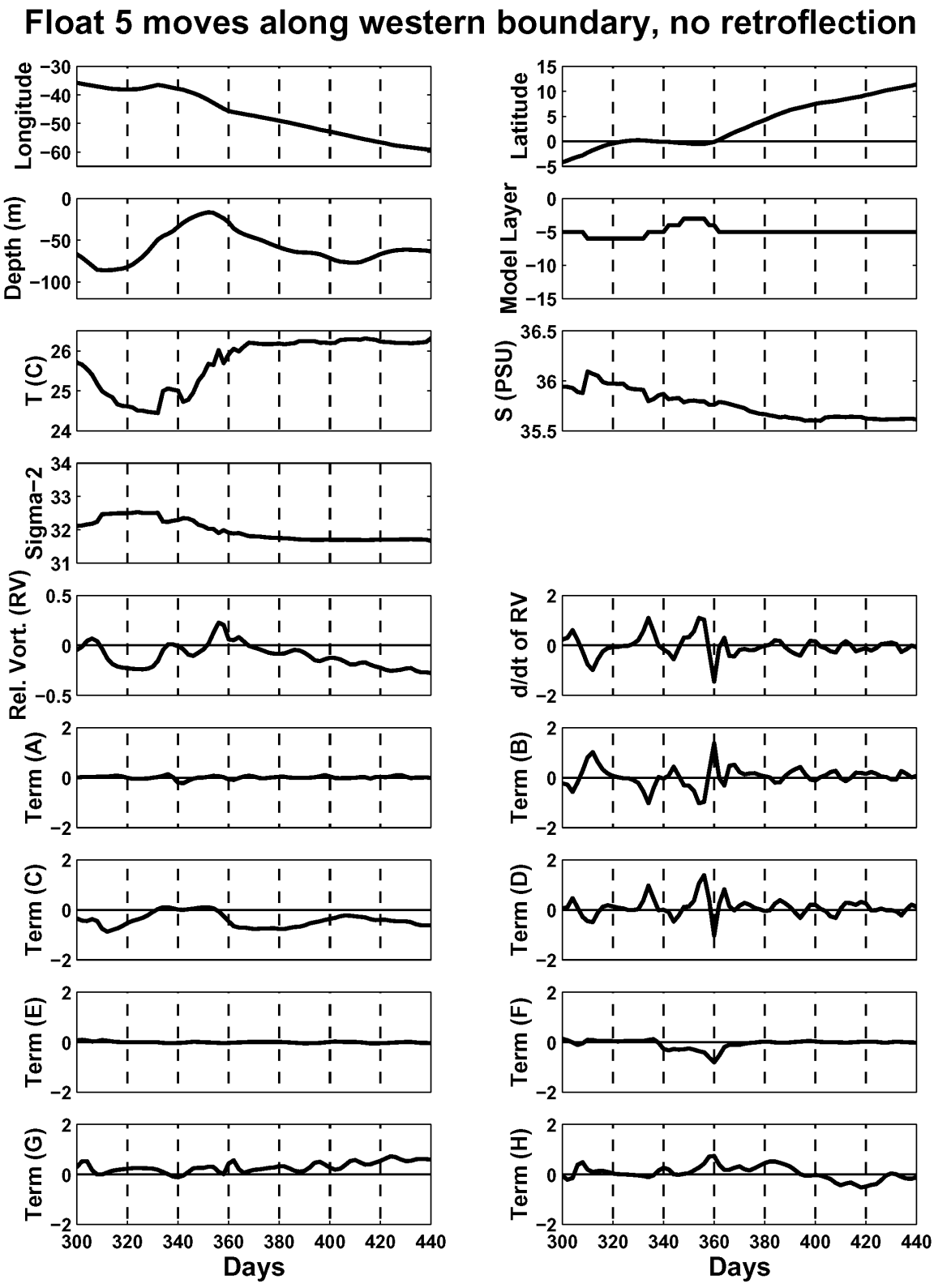

Figure 13f. Same as Figure 13a, but for a short segment along the path of float 5 when ir travels along the western boundary into the North Atlantic without retroflecting eastward.

terms. Because of the small values of these vorticity tendencies, this balance is almost impossible to see in Figure 13a. The float is heading southwest into a region of convergent isopycnals so the stretching term is accommodating conservation of potential vorticity as prescribed by layered thermocline theory [*Luyten et al,* 1983].

6.6. Float 5 travels along the western boundary.

Float 5 crosses the equator on the western side of the basin and then proceeds northwest along the western boundary directly towards the Caribbean without retroflecting into either the EUC or the NECC. We use this float to examine mechanisms associated with this more direct western boundary route, referring to Figure 13f for a segment of its history beginning on day 300. We begin with Float 5 located at about 65 m depth near the western boundary and south of the equator (much shallower than Float 1). The float deepens to 85 m as it approaches the equator, and then upwells to about 20 m while it resides on the equator. Relative vorticity is initially small and positive. It becomes larger and negative when the float reaches the equator (after day 410), largely because of planetary vorticity advection [term (C)], and it remains negative while the float resides on the equator. Different from Float 1, however, is the relative unimportance of the vortex stretching term as the float enters the equatorial region. Being above the EUC and thermocline it does not participate in the stretching associated with the EUC and hence does not generate sufficient relative vorticity to retroflect. While the float is at the equator several terms contribute to its Lagrangian vorticity tendency, but these tend to cancel one another.

After day 360, the float leaves the equator and moves northwestward along the western boundary past the NECC retroflection region. Relative vorticity gradually becomes more negative during this time, but it never grows to the large magnitude observed in Fig 13d by the time it passes the NECC retroflection region. Planetary vorticity advection is primarily responsible for the increase in negative vorticity, but both horizontal and vertical friction torques combine to limit the rate of negative vorticity generation and prevent retroflection. After day 390, the increase in negative vorticity is primarily countered by horizontal friction torque as a Munk boundary layer is established.

There are two key points associated with keeping this float attached to the western boundary. The first is its position near the surface where vertical friction torque can act (with the horizontal friction torque) to dissipate the generation of relative vorticity by planetary vorticity advection. The second is the float's crossover to the NEC side of the NECC trough prior to sufficient negative relative vorticity generation to facilitate a retroflection into the NECC. In other words, the NECC is not sufficiently developed when this float transits northwest along the western boundary to accommodate retroflection. Had it been present, the negative relative vorticity effect of stretching (compression by movement towards the NECC trough) would have facilitated retroflection by increasing negative relative vorticity and breaking the Munk layer constraint. Thus, floats positioned near the surface during the time of year (winter/spring)

when the surface dynamic topography associated with the equatorial and tropical gyres is relatively flat are able to proceed along the western boundary.

7. DISCUSSION

The HYCOM model, which uses an open-ocean vertical coordinate system that transitions from level (pressure) coordinates near the surface to isopycnic coordinates with increasing depth, is analyzed to study upper-limb pathways and mechanisms associated with the Atlantic Ocean's meridional overturning mode of circulation. The model domain extends from 30°S to 70°N on a 1.4-degree horizontal resolution grid with 25 vertical layers. Seasonally varying, climatological atmospheric fields are used to drive the model. The simulated Eulerian fields are similar in their overall attributes to those produced by other investigators using a variety of models. Our emphasis is on determining the three-dimensional Lagrangian pathways and the mechanisms by which these pathways are achieved as an analog to how they may occur in nature. Thus, we seed the model with Lagrangian floats, track these floats from their points of origin in the southern hemisphere subtropical gyre across the equator and across the equatorial and tropical gyres into the northern hemisphere subtropical gyre, and log the material property transformations that occur en route. Specific emphasis is on the vertical component of vorticity and how the various terms comprising the vorticity balance sum together locally to enable the floats to negotiate their individual treks.

The meridional overturning circulation is well represented, on average, with a zonally integrated strength of about 16 Sv in the subtropical North Atlantic. Approaching the equator from the south, the upper-limb shows northward flow within the thermocline and southward flow in the surface Ekman layer. A transition occurs in the vicinity of the equator where the thermocline waters upwell and are transported farther north in the surface Ekman layer. This is a well-known attribute described, for example, by *Roemmich* [1983]. What the pathways are, and how the water mass transformations occur, are questions that we begin to answer in the present study.

The system of seasonally varying wind-driven gyres are also well represented, as is the basic seasonal storage and release of internal energy associated with the gyres' dynamic topography. For instance, as in the z-coordinate model simulations of the seasonal cycle by *Philander and Pacanowski* [1986a; 1986b], we find a net northward internal energy flux by ocean currents into the NECC ridge in boreal spring/summer followed by a release of stored internal energy to the north in fall/winter.

How this works is one question that we set out to address. More generally, we have addressed how fluid manages to cross the equator and wend its way through the seasonally varying wind-driven gyres, and also through the subtropical overturning cells. From south to north, the wind-driven gyres consist of the anticyclonic southern hemisphere subtropical gyre, the clockwise equatorial gyre that straddles the equator, the cyclonic tropical gyre, and the

anticyclonic northern hemisphere subtropical gyre; these gyres being separated from one another by the zonally flowing (westward) SEC, (eastward) NECC, and (westward) NEC, respectively. Thermocline and lower surface layer water that approaches the equator from the south in the western boundary layer retroflects eastward into the EUC. This water warms and upwells into the westward-flowing SEC. The westward equatorial flow that reaches the western boundary then flows northwestward along the coast as the NBC.

Two different routes have been proposed for upper-limb flow within the NBC to reach the Caribbean Sea: 1) a western boundary current route, either directly [*Philander and Pacanowski,* 1986b] or within eddies [*Johns et al.,* 1993; *Barnier et al.*, 2001] and 2) an interior route [*Mayer and Weisberg,* 1993]. To highlight the Sverdrup streamfunction inconsistency with a direct western boundary current route, *Mayer and Weisberg* [1993] suggested the equatorial and tropical gyre naming and proffered a conceptual model of how the upper-limb pathways may negotiate these, with the seasonal cycle playing a fundamental role. Upper-limb flow enters the interior within the NECC during late spring through fall when internal energy is stored at that latitude. At this time of year, horizontal friction torque in the frictional western boundary layer (where Munk layer dynamics prevail) is not strong enough to offset negative vorticity generation in the NBC by planetary vorticity advection. This generation breaks the boundary layer constraint, allowing the fluid to retroflect toward the east. The subsequent winter release of the internal energy stored at this latitude is facilitated by a shift in the wind field that opens up the NEC trough, thereby allowing for vortex stretching and northward flow in the surface Ekman layer. This two-staged hypothesis, utilizing different physical mechanisms during different phases of the annual cycle, accommodates the requirements for water mass transformations and internal energy storage and release. It is also kinematically consistent with the cyclonic tropical gyre negating a strong northwestward boundary current as a continuous feature from the equator to the Caribbean. After advecting northward into the North Atlantic subtropical gyre, upper-limb fluid subducts and advects southward and westward, eventually entering the NEC and the Caribbean. After subduction, the flow is governed by layered thermocline theory.

This circuitous, upper-limb interior pathway hypothesis is what we set out to investigate by seeding the model with Lagrangian floats. The interior pathway is confirmed as a feature of the model's seasonal cycle. While somewhat more complex than surmised, it does account for a substantial fraction of the upper-limb northward heat flux. The importance of the set of five processes to interior pathways outlined in the Introduction is also confirmed. Rather than a few simple paths, however, most floats follow complicated paths typically involving multiple loops around gyres or in the North Atlantic subtropical overturning cell before proceeding farther north. Many floats also return to the southern hemisphere, either temporarily or permanently.

Common to all of the floats that are analyzed in some detail is that water property modifications are necessary for water parcels to negotiate their paths across the equator and between gyres. Equatorial upwelling appears to play a central role in this, as it should, since the northward meridional internal energy

flux increases across the equator by a factor of about 1.5 as water is upwelled and heated [*e.g., Bryden and Imawaki,* 2001]. Complementing the equatorial upwelling is downwelling farther north in the subtropical gyre where most of the floats undergo subduction prior to entering the Caribbean. Thus, the pathways are fully three-dimensional, non-isentropic, and time dependent, relying on seasonal shifts in the wind and surface buoyancy flux fields to set the stage for water parcel movements between gyres. A corollary finding is that neither isopycnic floats nor surface drifters are adequate to track upper-limb pathways from the subtropical South Atlantic to the subtropical North Atlantic in their entirety. Three-dimensional Lagrangian floats must be used, and since constructing such a float presupposes that we know a proper specification for mixing, they are presently not possible in nature. They can only be employed in models and are then subject to the uncertainties in the model's non-isentropic process parameterizations.

Depending on depth and location with respect to the phase of the seasonal cycle, floats can take a direct route to the Caribbean along the western boundary. For instance, floats along the western boundary near the surface in winter can flow directly into the Caribbean since the NECC is not developed during that time of year. The dynamic topography, by affecting the vortex stretching term, is instrumental in steering fluid parcels. When attached to the western boundary and with relatively flat dynamic topography in winter these floats are governed by a modified Munk boundary layer.

While our findings are sensible, a major shortcoming is that they result from a rather coarse resolution model that only marginally resolves the boundary layers of importance (the frictional and inertial boundary layers along the western boundary and the visco-inertial boundary layer along the equator). Nevertheless, the technique of tracking Lagrangian floats and diagnosing the material property variations en route, including thermodynamic (temperature and salinity) and dynamic (vorticity) properties, provides a useful tool for developing an understanding of the processes that control the meridional overturning mode of circulation

.

Acknowledgements

This work was initiated through support by the Office of Global Programs, National Oceanic and Atmospheric Administration, Grant number NA96GPO462. Informative discussions with Z. Garraffo, E. Chassignet, and A. Mariano of RSMAS; A. Wallcraft of the Naval Research Laboratory, and R. Bleck of Los Alamos National Laboratory are gratefully acknowledged. The authors thank W. Ebisuzaki of NOAA/NCEP for providing the NCEP/DOE reanalysis fields.

APPENDIX 1. DIAGNOSIS OF VERTICAL VELOCITY

The continuity equation in the HYCOM generalized vertical coordinate domain is

$$\frac{dw}{dp} = -\nabla_s \cdot \mathbf{v}, \tag{3}$$

where the subscripts indicate that the generalized vertical coordinate s is held constant during partial differentiation, and where vertical velocity is defined as

$$w = \frac{dp}{dt}. \tag{4}$$

The model consists of layers $k = 1,2,...,N$, with each layer k bounded by vertical coordinate surfaces located at pressure depths $p_k(x,y,s)$ above and $p_{k+1}(x,y,s)$ below. Since the HYCOM generalized coordinate system is not Cartesian, integration of (3) downward from the surface introduces additional terms related to the sloping s interfaces.

Integrating (3) downward from the surface where it is assumed that $w = 0$, and dropping the subscript s, the vertical velocity at the base of model layer $k = 1$ is

$$w(p_2^-) = -\int_{p_1}^{p_2^-}\left(\frac{\partial u}{\partial x} + \frac{\partial v}{\partial y}\right)dp = -(p_2^- - p_1)\left(\frac{\partial u_1}{\partial x} + \frac{\partial v_1}{\partial y}\right), \tag{5}$$

where the integration is carried out from the surface down to an infinitesimal distance above interface 2. To obtain the vertical velocity at the top of layer 2, the continuity equation is also integrated across interface 2 from p_2^- to p_2^+, which gives

$$w(p_2^+) = -(p_2 - p_1)\left(\frac{\partial u_1}{\partial x} + \frac{\partial v_1}{\partial y}\right) + (u_2 - u_1)\frac{\partial p_2}{\partial x} + (v_2 - v_1)\frac{\partial p_2}{\partial y}. \tag{6}$$

More generally, the vertical velocity at pressure P located within model layer n is

$$\begin{aligned} w(P) = &-\sum_{k=1}^{n-1}(p_{k+1} - p_k)\left(\frac{\partial u_k}{\partial x} + \frac{\partial v_k}{\partial y}\right) + q(p_{n+1} - p_n)\left(\frac{\partial u_n}{\partial x} + \frac{\partial v_n}{\partial y}\right) \\ &+\sum_{k=2}^{n}\left[(u_k - u_{k-1})\frac{\partial p_k}{\partial x} + (v_k - v_{k-1})\frac{\partial p_k}{\partial y}\right], \end{aligned} \tag{7}$$

where the first term on the right side is zero for $n = 1$, and where

$$P = p_n + q(p_{n+1} - p_n) \quad , \quad 0 < q < 1. \tag{8}$$

It is easy to show that

$$w(P) = w(p_n^+) + q[w(p_{n+1}^-) - w(p_n^+)]. \tag{9}$$

Thus, w varies linearly in the vertical within each model layer while discontinuities can exist at model interfaces.

Although w can be estimated directly from (7), a simpler expression can be derived by considering the HYCOM continuity (thickness tendency) equation. If subgrid-scale processes (thickness diffusion) are neglected, the time evolution of the thickness of model layer k is given by *Bleck* [2002]:

$$\left[\frac{\partial}{\partial t}(\Delta p_k)\right]_s = -\nabla_s \cdot (\mathbf{v}_k \Delta p_k) - \left(\dot{s}\frac{\partial p}{\partial s}\right)_{k+1} + \left(\dot{s}\frac{\partial p}{\partial s}\right)_k, \tag{10}$$

where $(\dot{s}\partial p/\partial s)_k$ is the entrainment velocity in pressure per unit time across interface k and s is held constant during partial differentiation. Assuming that the surface interface is stationary, integrating (10) downward from the surface to interface $n+1$ located at the base of layer n gives

$$\begin{aligned}\frac{\partial p_{n+1}}{\partial t} = &-\sum_{k=1}^{n}(p_{k+1} - p_k)\left(\frac{\partial u_k}{\partial x} + \frac{\partial v_k}{\partial y}\right) + \sum_{k=2}^{n}\left[(u_k - u_{k-1})\frac{\partial p_k}{\partial x} + (v_k - v_{k-1})\frac{\partial p_k}{\partial y}\right] \\ &-u_n\frac{\partial p_{n+1}}{\partial x} - v_n\frac{\partial p_{n+1}}{\partial y} - \left(\dot{s}\frac{\partial p}{\partial s}\right)_{n+1}.\end{aligned} \tag{11}$$

The interface vertical velocity vertically interpolated to pressure depth P within model layer n, with P given by (8), is

$$\begin{aligned}\frac{\partial P}{\partial t} = \frac{\partial p_n}{\partial t} + q\left(\frac{\partial p_{n+1}}{\partial t} - \frac{\partial p_n}{\partial t}\right) = &-\left\{\left(\dot{s}\frac{\partial p}{\partial s}\right)_n + q\left[\left(\dot{s}\frac{\partial p}{\partial s}\right)_{n+1} - \left(\dot{s}\frac{\partial p}{\partial s}\right)_n\right]\right\} \\ &-\sum_{k=1}^{n-1}(p_{k+1} - p_k)\left(\frac{\partial u_k}{\partial x} + \frac{\partial v_k}{\partial y}\right) + q(p_{n+1} - p_n)\left(\frac{\partial u_n}{\partial x} + \frac{\partial v_n}{\partial y}\right) \\ &+\sum_{k=2}^{n}\left[(u_k - u_{k-1})\frac{\partial p_k}{\partial x} + (v_k - v_{k-1})\frac{\partial p_k}{\partial y}\right] \\ &-u_n\left[\frac{\partial p_n}{\partial x} + q\left(\frac{\partial p_{n+1}}{\partial x} - \frac{\partial p_n}{\partial x}\right)\right] - v_n\left[\frac{\partial p_n}{\partial y} + q\left(\frac{\partial p_{n+1}}{\partial y} - \frac{\partial p_n}{\partial y}\right)\right].\end{aligned} \tag{12}$$

From (7), the third and fourth lines of (12) are identified as the fluid vertical velocity w at pressure depth P. As a result, (12) becomes

$$\begin{aligned}w(P) = \frac{\partial p_n}{\partial t} + q\left(\frac{\partial p_{n+1}}{\partial t} - \frac{\partial p_n}{\partial t}\right) + &\left\{\left(\dot{s}\frac{\partial p}{\partial s}\right)_n + q\left[\left(\dot{s}\frac{\partial p}{\partial s}\right)_{n+1} - \left(\dot{s}\frac{\partial p}{\partial s}\right)_n\right]\right\} \\ &+u_n\left[\frac{\partial p_n}{\partial x} + q\left(\frac{\partial p_{n+1}}{\partial x} - \frac{\partial p_n}{\partial x}\right)\right] + v_n\left[\frac{\partial p_n}{\partial y} + q\left(\frac{\partial p_{n+1}}{\partial y} - \frac{\partial p_n}{\partial y}\right)\right].\end{aligned} \tag{13}$$

The vertical velocity of model pressure interfaces can be separated as follows:

$$\frac{\partial p_k}{\partial t} = \frac{\partial \hat{p}_k}{\partial t} - \left(\dot{s} \frac{\partial p}{\partial s} \right)_k . \tag{14}$$

If the entrainment velocity is zero, the interface vertical velocity equals $\partial \hat{p}_k / \partial t$, which can therefore be interpreted as the local vertical velocity of a material surface. Substituting (14) into (13),

$$\begin{aligned} w(P) = {} & \frac{\partial \hat{p}_n}{\partial t} + q\left(\frac{\partial \hat{p}_{n+1}}{\partial t} - \frac{\partial \hat{p}_n}{\partial t} \right) \\ & + u_n \left[\frac{\partial p_n}{\partial x} + q\left(\frac{\partial p_{n+1}}{\partial x} - \frac{\partial p_n}{\partial x} \right) \right] + v_n \left[\frac{\partial p_n}{\partial y} + q\left(\frac{\partial p_{n+1}}{\partial y} - \frac{\partial p_n}{\partial y} \right) \right]. \end{aligned} \tag{15}$$

The first term on the right side of (15) is the vertically interpolated material surface vertical velocity. The other two terms on the right side represent the vertical component of layer k flow parallel to sloping interfaces. The vertical velocity at the top and bottom of layer n are obtained by setting $q = 0$ and $q = 1$, respectively:

$$\begin{aligned} w(p_n^+) &= \frac{\partial \hat{p}_n}{\partial t} + u_n \left(\frac{\partial p_n}{\partial x} \right) + v_n \left(\frac{\partial p_n}{\partial y} \right) \\ w(p_{n+1}^-) &= \frac{\partial \hat{p}_{n+1}}{\partial t} + u_n \left(\frac{\partial p_{n+1}}{\partial x} \right) + v_n \left(\frac{\partial p_{n+1}}{\partial y} \right) \end{aligned} . \tag{16}$$

The first step in estimating w for float advection is to calculate three-dimensional fields of $w(p_n^+)$ and $w(p_{n+1}^-)$. The vertical velocity is then estimated at the location of each float using the procedures described in Appendix 2.

APPENDIX 2. SPATIAL INTERPOLATION OF MODEL VARIABLES TO FLOATS

To interpolate variables stored on the HYCOM generalized coordinate system to float locations, the first step is to identify the model layer that contains the float. It is initially assumed to be in the same model layer that it was in during the previous time step. The sixteen pressure grid points surrounding the float are then selected. Land points are masked from the interpolation, as are points where the layer containing the float has collapsed to zero thickness at the bottom. If a sufficient number of surrounding grid points remain, a two-dimensional polynomial surface is fit to the data to perform the interpolation using the same routine that *Mariano and Brown* [1992] employed for the large-scale trend surface fit in their parameter matrix objective analysis algorithm. If too few surrounding grid points remain, a bilinear scheme using the four surrounding grid points is invoked to perform the interpolation. If only one point

remains, field values at that point are assigned to the float location. If the situation arises where no grid points remain, the float is assumed to have run aground. If the three-dimensional velocity field is perfectly known at the float location, this situation should never arise. However, the model grid poorly resolves the topography in coastal regions, and model fields must be extrapolated to floats located at the immediate coast. The relatively large interpolation errors at the coast cause some floats to run aground. Despite this problem, the large majority of floats never run aground. Of floats that follow the interior upper-limb pathway, none of them run aground before entering the Caribbean Sea.

With the float initially assumed to be in model layer n, the pressure depths of model interfaces n and $n+1$ are each horizontally interpolated to the float location. If the pressure depth of the float is no longer located between p_n and p_{n+1}, the new layer containing the float is identified. Other model variables are then interpolated to the float location. These variables are interpolated from their native grid (p for thermodynamical variables, u for zonal velocity, v for meridional velocity, or q for vorticity) on the Arakawa C-mesh. As a result, the grid box selection procedure described above is repeated for each of these grids. Horizontal interpolation of interface pressure and of model layer variables to a float is straightforward because it is values at the surrounding grid points that are interpolated. A different procedure is required for vertical velocity, which from (9) varies linearly with depth within the layer. It is first necessary to vertically interpolate $w(p_n^+)$ and $w(p_{n+1}^-)$ from (16) at the surrounding grid points as follows: Given a float located at pressure P within model layer n, the quotient q is determined at the float location using (8) after interpolating p_n and p_{n+1} from the surrounding points:

$$q = \frac{P - p_n}{p_{n+1} - p_n}. \tag{17}$$

The vertically interpolated value of w at each surrounding grid point is then estimated using

$$w = q w(p_n^+) + (1-q)\, w(p_{n+1}^-), \tag{18}$$

and it is these w values that are horizontally interpolated to the float location.

APPENDIX 3. FLOAT ADVECTION

The fourth-order Runga-Kutta algorithm used to temporally interpolate velocity for float advection is a well-known procedure that is commonly used for synthetic floats and drifters in other models [e.g. *Malanotte-Rizzoli et al.*, 2000]. The procedure requires estimates of the model velocity at the present time and at two earlier times. If three-dimensional Lagrangian floats are selected, the time interpolation is performed for all three velocity components; otherwise, it is performed only on the horizontal velocity components. Ideally, the time interval

separating each of the velocity component fields used in the interpolation should be between one and two hours, a criterion obtained from the MICOM float experience [*Garraffo et al.*, 2001a; 2001b].

The model baroclinic time interval Δt_{bc} is set prior to starting the model run. The velocity sampling time interval is set to an integer number of baroclinic time steps ($\Delta t_{vel} = n_{vel} \Delta t_{bc}$). The float is then advected every $2n_{vel} \Delta t_{bc}$ time intervals. When HYCOM is run at low horizontal resolution, Δt_{bc} is typically about one hour, so n_{vel} is typically set to 2. (In the present study, these values are set to 1/20 day and 2, respectively so that floats are advected five times per day.) When HYCOM is run at high horizontal resolution, Δt_{bc} is substantially less than one hour. In this case, n_{vel} is set to a value that insures that Δt_{vel} is between one and two hours. With this selection made, the float is advected using fields at the present time and at the two earlier times $t - n_{vel} \Delta t_{bc}$ and $t - 2n_{vel} \Delta t_{bc}$. When the HYCOM float subroutine is called at intermediate times, it only saves the u, v, and w fields required for the next time interpolation. Time series of float location and model variables are output every two days for analysis. Interpolation of water properties to the float location is performed only at these output time steps.

For isopycnic and isobaric floats, w is not estimated or interpolated to float locations. If isopycnic floats are selected, the depth of each float is set to the vertically interpolated depth of the reference isopycnic surface after horizontal advection is performed. For isobaric floats, of course, the pressure depth is not changed.

REFERENCES

Barnier, B., T. Reynauld, A. Beckmann, C. Boning, J-M Molines, S. Barnard, and Y. Jia, On the seasonal variability and eddies in the North Brazil Current: insights from model intercomparison experiments, *Prog. Oceanogr.*, *48*, 195-230, 2001.

Blanke, B., M. Arhan, G. Madec, and S. Roche, Warm water paths in the equatorial Atlantic as diagnosed with a general circulation model, *J. Phys. Oceanogr.*, *29*, 2753-2768, 1999.

Bleck, R., An oceanic general circulation model framed in hybrid isopycnic-Cartesian coordinates, *Ocean Modeling*, *4*, 55-88, 2002.

Bleck, R. and D. B. Boudra, Initial testing of a numerical ocean circulation model using a hybrid (quasi-isopycnic) vertical coordinate, *J. Phys. Oceanogr.*, *11*, 755-770., 1981.

Boudra, D. B. and E. P. Chassignet, Dynamics of Agulhas retroflection and ring formation in a numerical model. Part I: The vorticity balance, *J. Phys. Oceanogr.*, *18*, 280-303, 1988.

Bryden, H.L. and S. Imawaki, Ocean heat transport, in *Ocean Circulation and Climate,* G. Siedler, J. Church, and J. Gould, eds., Academic Press, San Diego, CA., 455-474, 2001.

Charney, J. G. and S. L. Spiegel, Structure of wind-driven equatorial currents in homogeneous oceans, *J. Phys. Oceanogr.*, *1*, 149-160, 1971.

Fratantoni, D. M., On the pathways and mechanisms of upper-ocean mass transport in the tropical Atlantic Ocean, Ph.D. Dissertation, *RSMAS Technical Report 96-006*, University of Miami, Miami, FL, 247pp., 1996.

Fratantoni, D. M., W. E. Johns, T. L. Townsend, and H. E. Hurlburt, Low-latitude circulation and water mass transport in a model of the tropical Atlantic Ocean, *J. Phys. Oceanogr.*, *30*, 1944-1966, 2000.

Garraffo, Z., D. A. J. Mariano, A. Griffa, C. Veneziani, and E. P. Chassignet, Lagrangian data in a high resolution numerical simulation of the North Atlantic. I: Comparison with *in-situ* float data, *J. Mar. Sys., 29*, 157-176, 2001a.

Garraffo, Z. D., A. Griffa, A. J. Mariano, and E. P. Chassignet, Lagrangian data in a high resolution numerical simulation of the North Atlantic. II: On the pseudo-Eulerian averaging of Lagrangian data, *J. Mar. Sys.*, *29*, 177-200, 2001b.

Garzoli, S.L. and E.J. Katz, The forced annual reversal of the Atlantic North Equatorial Countercurrent, *J. Phys. Oceanogr.*, *13*, 2082-2090, 1983.

Haidvogel, D. B., On the feasibility of particle tracking in Eulerian ocean models, *Ocean Modelling, 45*, 4-9, 1982.

Halliwell, Jr. G. R., Evaluation of vertical coordinate and vertical mixing algorithms in the hybrid-coordinate ocean model (HYCOM), submitted to *Ocean Modeling,* 2003.

Harper, S., Thermocline ventilation and pathways of tropical-subtropical water mass exchange, *Tellus, 52A*, 330-345, 2000.

Inui, T., A. Lazar, P Malanotte-Rizzoli, and A. Busalacchi, Wind stress effects on subsurface pathways from the subtropical to tropical Atlantic, *J. Phys. Oceanogr.*, *32*, 2257-2276, 2002.

Johns, W.E., T.N. Lee, F. Schott, R.J. Zantopp, and R. Evans, The North Brazil Current retroflection: seasonal structure and eddy variability, *J. Geophys. Res.*, *95*, 22103-22120, 1993.

Kalnay, *et al*., The NCEP/NCAR 40-year reanalysis project, *Bull. Amer. Meteorol. Soc*., *77*, 437-471, 1996.

Kanamitsu, M., W. Ebisuzaki, J. Woollen, S-K Yang, J. J. Hnilo, M. Fiorino, and G. L. Potter, Ncep-Doe AMIP-II Reanalysis (R-2), *Bull. Amer. Meteorol. Soc.*, *83*, 1631-1643, 2002.

Kara, A. B., P. A. Rochford, and H. E. Hurlburt, Efficient and accurate bulk parameterizations of air-sea fluxes for use in general circulation models, *J. Atmos. Oceanic Technol.*, *17*, 1421-1438, 2000a.

Kara, A. B., P. A. Rochford, and H. E. Hurlburt, An optimal definition for ocean mixed layer depth, *J. Geophys. Res.*, *105*, 16803-16821, 2000b.

Katz, E. J., Seasonal response of the sea surface to the wind in the equatorial Atlantic, *J. Geophys. Res.*, *92*, 1885-1893, 1987.

Large, W. G., J. C. Mc Williams, and S. C. Doney, Oceanic vertical mixing: a review and a model with a nonlocal boundary layer parameterization, *Rev. Geophys. 32*, 363-403, 1994.

Lazar, A., T. Inui, P. Malanotte-Rizzoli, A. J. Busalacchi, L. Wang, and R. Murtugudde, Seasonality of the ventilation of the tropical Atlantic thermocline in an OGCM, *J. Geophys. Res.*, in press, 2003.

Levitus, S. and T. Boyer, *World Ocean Atlas 1994 Volume 4: Temperature*, NOAA Atlas NESDIS 4, U.S. Department of Commerce, Washington, D.C., 1994.

Levitus, S., R. Burgett, and T. Boyer, *World Ocean Atlas 1994 Volume 3: Salinity*, NOAA Atlas NESDIS 3, U.S. Department of Commerce, Washington, D.C., 1994.

Luyten, J.R., J. Pedlosky, and H. Stommel, The ventilated thermocline, *J. Phys. Oceanogr.*, *13*, 292-309, 1983.

Malanotte-Rizzoli, P., K. Hedstrom, H Arango, and D. B. Haidvogel, Water mass pathways between the subtropical and tropical ocean in a climatological simulation of the North Atlantic ocean circulation, *Dyn. Atmos. Oceans*, *32*, 331-371, 2000.

Mariano, A. J. and O. B. Brown, Efficient objective analysis of dynamically heterogeneous and nonstationary fields via the parameter matrix, *Deep Sea Res.*, *39*, 1255-1292, 1992.

Mayer, D. A. and R. H. Weisberg, A description of COADS surface meteorological fields and the implied Sverdrup transports for the Atlantic Ocean from 30°S to 60°N, *J. Phys. Oceanogr.*, *23*, 2201-2221, 1993.

Munk, W.H., On the wind-driven ocean circulation, *J. Meteor.*, *7*, 79-93, 1950.

Philander, S. G. H. and R. C. Pacanowski, A model of the seasonal cycle in the tropical Atlantic Ocean, *J. Geophys. Res.*, *91*, 14,192-14,206, 1986a.

Philander, S. G. H. and R. C. Pacanowski, The mass and heat budget in a model of the tropical Atlantic Ocean, *J. Geophys. Res., 91*, 14,212-14,220, 1986b.

Roemmich, D. H., The balance of geostrophic and Ekman transports in the tropical Atlantic Ocean, *J. Phys. Oceanogr., 13*, 1534-1539, 1983.

Schmitz, W.J. and P.L. Richardson, On the sources of the Florida Current, *Deep-Sea Res.*, *38* (Suppl. 1), S379-S409, 1991.

Schmitz, W.J. and M.S. McCartney, On the North Atlantic circulation, *Rev. Geophys.*, *31*, 29-49, 1993.

Schott, F. A., J. Fischer, and L. Stramma, Transports and pathways of the upper-layer circulation in the western tropical Atlantic, *J. Phys. Oceanogr., 28*, 1904-1928, 1998.

Sun, S., R. Bleck, C. G. H. Rooth, J. Dukowicz, E. P. Chassignet, and P. Killworth, Inclusion of thermobaricity in isopycnic-coordinate ocean models, *J. Phys. Oceanogr., 29*, 2719-2729, 1999.

Weisberg, R.H. and T.J. Weingartner, Instability waves in the equatorial Atlantic Ocean, *J. Phys. Oceanogr., 18*, 1641-1657, 1988.

Weisberg and Qiao, Equatorial upwelling in the central Pacific estimated from moored velocity profilers, *J. Phys. Oceanogr., 30*, 105-124, 2000.